KTH Engineering Sciences

Short Pulses in Engineered Nonlinear Media

STEFAN HOLMGREN

Doctoral Thesis

Department of Applied Physics
Royal Institute of Technology
Stockholm, Sweden 2006

Royal Institute of Technology
Department of Applied Physics - Laser Physics
AlbaNova
Roslagstullsbacken 21
SE-106 91 Stockholm, Sweden

Akademisk avhandling som med tillstånd av Kungliga Tekniska Högskolan framlägges till offentlig granskning för avläggande av teknologie doktorsexamen i fysik, måndagen den 18 december 2006, kl. 10.15 i Sal FD5, AlbaNova, Roslagstullsbacken 21, Stockholm. Avhandlingen kommer att försvaras på engelska.

TRITA-FYS 2006:74
ISSN 0280-316X
ISRN KTH/FYS/--06:74--SE

ISBN 978-91-7178-540-4
ISBN 91-7178-540-X

Cover picture: Čerenkov FROG trace.

Printed by Universitetsservice AB, Stockholm 2006.

Stefan Holmgren
Short Pulses in Engineered Nonlinear Media
Department of Applied Physics - Laser Physics,
Royal Institute of Technology,
SE-106 91 Stockholm, Sweden

Abstract

Short optical pulses and engineered nonlinear media is a powerful combination. Mode locked pulses exhibit high peak powers and short pulse duration and the engineered ferro-electric $KTiOPO_4$ facilitates several different nonlinear processes. In this work we investigate the use of structured, second-order materials for generation, characterization and frequency conversion of short optical pulses.

By cascading second harmonic generation and difference frequency generation the optical Kerr effect was emulated and two different Nd-based laser cavities were mode locked by the cascaded Kerr lensing effect. In one of the cavities 2.8 ps short pulses were generated and a strong pulse shortening took place through the interplay of the cavity design and the group velocity mismatch in the nonlinear crystal. The other laser had a hybrid mode locking scheme with active electro-optic modulation and passive cascaded Kerr lensing incorporated in a single partially poled KTP crystal. The long pulses from the active modulation were shortened when the passive mode locking started and 6.9 ps short pulses were generated.

High-efficiency frequency conversion is not a trivial task in periodically poled materials for short pulses due to the large group velocity mismatch. Optimization of parameters such as the focussing condition and the crystal temperature allowed us to demonstrate 64% conversion efficiency by frequency doubling the fs pulses from a Yb:KYW laser in a single pass configuration. Quasi phase matching also offers new possibilities for nonlinear interactions. We demonstrated that it is possible to simultaneously utilize several phase matched second harmonic interactions, resulting in a dual-polarization second harmonic beam.

Short pulse duration of the fundamental wave is a key parameter in the novel method that we demonstrated for characterization of the nonlinearity of periodically poled crystals. The method utilizes the group velocity mismatch between the two polarizations in a type II second harmonic generation configuration.

The domain walls of PPKTP exhibit second order nonlinearities that are forbidden in the bulk material. This we used in a single shot frequency resolved optical gating arrangement. The spectral resolution came from Čerenkov phase matching, a non-collinear phase matching scheme that exhibits a substantial angular dispersion. The second harmonic light was imaged upon a CCD camera and with the spectral distribution on one axis and the temporal autocorrelation on the other. From this image we retrieved the full temporal profile of the fundamental pulse, as well as the phase. The spectral dispersion provided by the Čerenkov phase matching was large enough to characterize optical pulses as long as ~200 fs in a compact setup. The Čerenkov frequency resolved optical gating method samples a thin stripe of the beam, i.e. the area close to the domain wall. This provides the means for high spatial resolution measurements of the spectral-temporal characteristics of ultrafast optical fields.

Keywords: nonlinear optics, KTiOPO4, frequency conversion, mode-locked lasers, ultra-fast lasers, visible lasers, short pulses, ultrafast nonlinear optics, diagnostic applications of nonlinear optics, nonlinear optical materials,

"Qu. 26. Have not the Rays of Light several sides, endued with several original Properties?"
- Isaac Newton, Opticks, 2nd ed. 1717

List of Publications

Publications included in the thesis

I. S. J. Holmgren, V. Pasiskevicius, and F. Laurell, *Generation of 2.8 ps pulses by mode-locking a Nd:$GdVO_4$ laser with defocusing cascaded Kerr lensing in periodically poled KTP*, Optics Express **13**, 5270-5278 (2005)

II. S. J. Holmgren, A. Fragemann, V. Pasiskevicius, and F. Laurell, *Active and passive hybrid mode-locking of a Nd:YVO_4 laser with a single partially poled KTP crystal*, Optics Express **14**, 6675-6680 (2006)

III. A. A. Lagatsky, C. T. A. Brown, W. Sibbett, S. J. Holmgren, C. Canalias, V. Pasiskevicius, and F. Laurell, *Efficient Doubling of Femtosecond Pulses in Aperiodically and Periodically Poled KTP Crystals*, Optics Express (submitted)

IV. V. Pasiskevicius, S. J. Holmgren, S. Wang, and F. Laurell, *Simultaneous second-harmonic generation with two orthogonal polarization states in periodically poled KTP*, Optics Letters **27**, 1628-1630 (2002)

V. S. J. Holmgren, V. Pasiskevicius, S. Wang, and F. Laurell, *Three-dimensional characterization of the effective second-order nonlinearity in periodically poled crystals*, Optics Letters **28**, 1555-1557 (2003)

VI. S. J. Holmgren, C. Canalias, and V. Pasiskevicius, *Ultrashort single-shot pulse characterization with high spatial resolution using localized nonlinearities in ferroelectric domain walls*, Optics Letters (submitted)

Publications not included in thesis

A. S. J. Holmgren, V. Pasiskevicius, and F. Laurell, *Generation of 2.8 ps pulses by mode-locking a Nd:$GdVO_4$ laser with defocusing cascaded nonlinearity in periodically poled KTP*, OSA Trends in Optics and Photonics **98**, ASSP 2005, 669-673, (2005).

B. V. Pasiskevicius, S. J. Holmgren, S. Wang, and F. Laurell, *3D-mapping of effective second-order nonlinearity in periodically poled crystals*, OSA Trends in Optics and Photonics **83**, ASSP 2003, 254-258 (2003).

C. J. H. Garcia-Lopez, V. Aboites, A. V. Kir'yanov, S. Holmgren, and M. J. Damzen, *Experimental study and modelling of a diode-side-pumped Nd:YVO_4 laser*, Optics Communications **201**, 425-430 (2002)

D. J. H. Garcia-Lopez, V. Aboites, A. V. Kir'yanov, S. Holmgren, and M. J. Damzen, *Experimental study and modelling of a diode-side-pumped Nd: YVO_4 laser*, Proc. SPIE **4595**, 310-318 (2001)

Acknowledgements

First of all I want to thank the two persons that have had the greatest impact on this thesis – Professor Fredrik Laurell and Dr. Valdas Pasiskevicius. Fredrik granted me this stimulating position and has supported me ever since. Valdas is a wizard in the lab and has a never ending list of fun experiments to perform. I am proud to have been working with you!

I would like to mention my past and present room mates – Rosalie Clemens, Jonas Hellström, Markus Alm and Carlota Canalias. Thanks for good laughs, friendship and a relaxed atmosphere!

To the other past and present members of the group – for lunch-time discussions, conference travels and fun parties. Agneta Falk, Björn Jacobsson, Gunnar Karlsson, Jens Tellefsen, Jonas Hellström, Junji Hirohashi, Lars-Gunnar Andersson, Mikael Tiihonen, Pär Jelger, Sandra Johansson, Shunhua Wang, Stefan Bjurshagen, Stefan Spiekermann – thanks for making my stay here so pleasant!

I was fortunate to have the opportunity to teach. My collegues in the lecture halls: Peter Unsbo, Göran Manneberg, Linda Lundström, Jessica Hultström, Per Takman and Heide Stollberg – it was a pleasure working with you!

Thanks to Ara Minassian and Mike Damzen, Imperial College, for showing me how fun laboratory work can be a time when I needed to be reminded. Alexander Lagatsky and Edik Rafailov, for making my two weeks in Scotland the start of such an enjoyable and fruitful collaboration.

I am grateful to the Royal Intitute of Technology for providing my salary, Göran Gustafsson's Foundation and Carl Trygger's Foundation for being able to buy equipment, Ragnar and Astrid Signeul's Foundation as well as Knut and Alice Wallenberg's Foundation for travel grants. Without funding there would be very little science indeed.

Outside work my special thanks to:

The Holmgren Clan: Aina & Bertil, my brothers Lars, Olov and Erik with their loved ones. Thanks for caring so immensely about me.

Anna Burvall – for being my friend all the way through. And for the fun of designing the new Optical Design course.

Erik Johansson and Mattias Sandström, for being good solid friends and for the great time I have had in your homes.

My dear friends around the Stockholm area – for all the small gatherings indoors and outdoors. My floorball playing friends – thanks for the fun at and outside the court.

Finally, all my love to my fiancé Jessica Karlsson. You make me a happy man!

Contents

Chapter 1

Introduction

1.1 Thesis outline

The thesis work is about mode locked laser pulses and engineered nonlinear media. A more detailed description would be that it concerns the generation, use, and characterization of mode locked pulses and that is achieved in engineered potassium titanyl phosphate (KTP). In the original research work we generate short pulses by the use of intracavity elements of periodically poled KTP. There are many uses for short pulses in combination with periodically poled media. We demonstrate efficient frequency doubling, three-dimensional characterization of nonlinear crystals and the simultaneous generation of second harmonic light of orthogonal polarizations. We also demonstrate that the nonlinearity at domain walls can be utilized for temporal (intensity and phase) and spatial characterization of short pulses.

In this introductory chapter the concept of a laser is described, followed by the description of laser beams and short optical pulses. Chapter two involves some brief laser theory and the principles of mode locking a laser. In the third chapter the basic theory of nonlinear optics is derived, starting from Maxwell's equations and ending with the concept of phase matching. The fourth chapter contains all the experiments mentioned above and some related theory. The thesis is concluded by the summary in chapter five and by the description of the author's contribution to the research work found in chapter six.

1.2 Introduction to lasers

The word laser is an acronym, standing for Light Amplification by Stimulated Emission of Radiation. The laser is a source of coherent electromagnetic radiation in the optical wavelength region, which ranges from several hundred μm for far infrared lasers to a few nm for soft x-ray lasers. In between these extremes are the more common lasers in the near infrared, in the visible and in the ultra violet spectral regions.

Laser light is coherent electromagnetic radiation and it differs from the light of black bodies like the sun or a light bulb in several ways. Some of these are the coherence property, the directionality, the brightness, the monochromaticity and the possibility of ultrashort pulses. The most fundamental difference is that of coherence, both temporal and spatial. A simple description of spatial coherence is a fixed phase relation between two points P_1 and P_2 on the wave front if P_2 lies within the coherence area around P_1. In the same way, temporal coherence can be described as the existence of a fixed relation between the phase at a point at one moment and the phase at the same point at any other time within the coherence time. The formal definitions of coherence shows that both coherence time and coherence area are statistical entities[1] defined from the normalized mutual coherence function but in this treatise the descriptions above are sufficient.

A direct consequence of the spatial coherence is the directionality property. Even a laser beam will spread due to diffraction, see paragraph 1.4. According to Huygens's principle the wave front at a distance can be obtained by the coherent superposition of wavelets emitted at an aperture. With a source of limited spatial coherence, the limiting aperture for coherent superposition is then the coherence area and thus the light from an incoherent light source will spread much more than that from a laser.

A related property is that of brightness, defined as power emitted per unit area and unit solid angle. The brightness of a laser of moderate power, e.g. a few milliwatts, can be as bright as the best conventional light source available. The brightness is the only reason why lasers are more dangerous than conventional light sources. This is because a laser beam can be focussed down to spot sizes of in the order of 1 μm, thus rendering extreme intensities.

The temporal coherence is the reason for the monochromaticity of lasers.

For reasons described later on, lasers are able to emit their power in the form of short pulses, with pulse lengths down to a few fs. This is achieved through the process of mode locking, which will be described in detail in section 2.3. The peak powers of a pulsed laser system can be enormous, and the applications are numerous.

Before the first laser was built, the microwave equivalent was realised by Townes *et al*. in 1958.[2,3] The transition from microwave to optical wavelengths was not trivial and challenges as well as possibilities were summarized by Schawlow and Townes in 1958.[4] Then an intense race for constructing the first working laser followed until Maiman[5] could announce the advent of the ruby laser in 1960. A new field in physics was born and during the first five years a plethora of fundamental laser types and modes of operation were discovered including, but not limited to, continuous wave (CW) lasing[6], gas lasers[7], semi-conductor lasers[8], fibre laser amplifiers[9], mode locked lasers[10], q-switched lasers[11], frequency conversion[12] etc.[13]

1.3 A schematic laser

In this chapter a limited theory of lasers is presented, for a more thorough description there are excellent textbooks available.[14,15,16,17,18] A working laser has three fundamental components, namely an active media, a pumping process and a feedback mechanism. A schematic laser is shown in fig. 1.1. The active media contains atoms or molecules in which the process of stimulated emission takes place. The actual media can be a gas, a plasma, a liquid or solids including glass, crystals and semi-conductors. The pumping process is a means of providing the active media with energy and this can be in the form of photons from a flash lamp or a diode laser, by direct electrical current or by gas discharges, to mention the most common ways. The feedback usually comes from mirrors or Fresnel reflections. More details on how lasers in general and mode locked lasers in particular work are given in chapter 2.

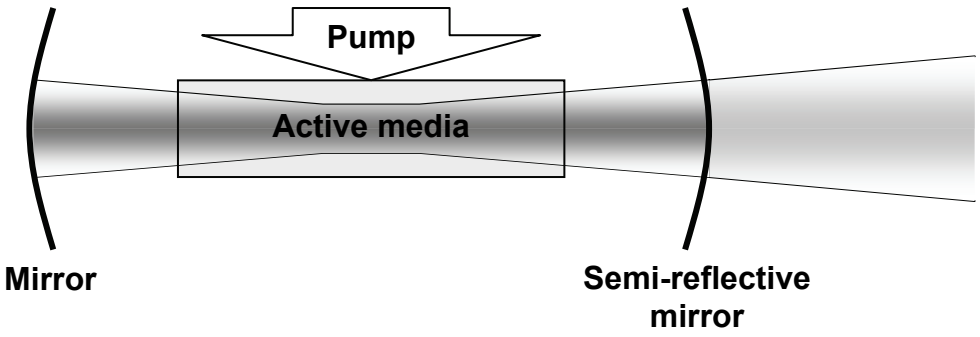

Figure 1.1. A schematic laser. The mirrors provide feedback.

1.4 Gaussian beams

This thesis deals with coherent light generated in laser resonators. The electromagnetic modes that can be sustained in a laser with cylindrical symmetry have a Gaussian transversal intensity distribution. The existence of eigen-modes in resonators with open sides was not obvious when Fox and Li did the first computer based numerical calculations, letting a plane wave bounce back and fourth in between two plane mirrors, calculating diffraction and looking for convergence in the shape of the wave.[19]

The beams from stable laser resonators are approximately Gaussian in transverse intensity distribution. Gaussian beams are exact solutions to the paraxial wave equation[20] and can be focussed with cone angles up to ≈ 30° before correction terms become necessary.[15]

The full vectorial polarization driven wave equation (eq.3.22), valid for both linear and nonlinear optics is derived in chapter 3. In this scalar treatment we assume that the temporal and spatial dependency of the electric field can be separated. This means that the wave equation can then be separated into a temporal and a spatial part. Assuming that the wave is monochromatic with an angular frequency of ω, the following general electric field satisfies the temporal wave equation:

$$\tilde{E}(x,y,z,t) = \tfrac{1}{2}\left[E(x,y,z)exp(-i\omega t) + c.c.\right] \qquad 1.1$$

Here and in the following the tilde sign (~) stands for a rapidly varying field. The complex notation is mathematically convenient, but a physical electric field is a real-valued entity. The spatial wave equation is known as Helmholtz equation and it has the following form in isotropic media:

$$\left[\nabla^2 + k^2\right]E(x,y,z) = 0 \qquad 1.2$$

Here k is the wave vector. The two most well known solutions to equation 1.2 are the plane wave and the spherical wave. Neither of them is good at describing a laser beam, though. A laser beam has the directional property of a plane wave and the curved phase front of a spherical wave. Furthermore, it has a very limited spatial extent and therefore the analysis can be restricted to paraxial waves propagating in the z direction:

$$E(x,y,z) = A(x,y,z)exp(ikz) \qquad 1.3$$

The Helmholtz equation can then be reduced to the paraxial form of equation 1.4 under the paraxial approximation of equation 1.5:

$$\left[\nabla_\perp^2 + i2k\frac{\partial}{\partial z}\right]A(x,y,z) = 0 \qquad 1.4$$

$$\left|\frac{\partial^2 A}{\partial z^2}\right| << \left|2k\frac{\partial A}{\partial z}\right| \qquad 1.5$$

The $\perp$ symbol denotes transversal derivative. One solution to the paraxial Helmholtz equation is given by a spherical wave with a complex radius of curvature q:

$$A(x,y,z) = A_0 \frac{q_0}{q(z)} exp\left(-ik\frac{x^2+y^2}{2q(z)}\right) \quad 1.6$$

Here A_0 denotes the field at origo and q_0 is short for $q(0)$. Equation 1.6 is the Gaussian beam solution, but in order to see the significance, q, or rather the inverse of q needs to be written in physically relevant parameters. The inverse of the complex radius of curvature can be divided into a real and an imaginary part.

$$\frac{1}{q(z)} = \frac{1}{R(z)} + i\frac{\lambda}{\pi w^2(z)} \quad 1.7$$

$R(z)$ is the phase front radius and w is the beam radius at the point where the intensity has dropped to $1/e^2$ of the on-axis value. Assume that the beam waist is at z = 0, where the radius if curvature thus is infinity. The beam radius at the waist is then w_0, where after it is w(z). By introducing the Rayleigh length, z_R, which is the distance by which the beam has doubled its area, a set of simple equations for the beam size and phase front curvature can be introduced:

$$z_R = \frac{\pi w_0^2}{\lambda} \quad 1.8$$

$$R(z) = z + \frac{z_R^2}{z} \quad 1.9$$

$$w(z) = w_0\sqrt{1+\left(\frac{z}{z_R}\right)^2} \quad 1.10$$

Another commonly used measure of the depth of focus is the confocal parameter, b, which is equal to twice the Rayleigh length. The beam radius is a hyperbola with the asymptotic angle θ, which is the far field half angle:

$$\theta = \lim_{z\to\infty}\frac{w(z)}{z} = \frac{w_0}{z_R} = \frac{\lambda}{\pi w_0} \quad 1.11$$

For a more informative version of equation 1.6, the use of algebra and the equations 1.7-1.10 leads to the following relation:

$$A(x,y,z) = A_0 \cdot \frac{w_0}{w(z)} \cdot exp\left(-arctan\left(\frac{z}{z_R}\right)\right) \cdot exp\left(ik\frac{x^2+y^2}{2R(z)}\right) \cdot exp\left(-\frac{x^2+y^2}{w^2(z)}\right) \quad 1.12$$

The first term represents the amplitude of the field at origo, the second term the transversal scaling necessary for maintaining a constant power in the beam, the third term is the Gouy phase – an additional phase change of π that occurs when passing through a focus, the fourth represents the curved phase front, and the fifth the Gaussian field strength variation. Remember that to see the full temporal and spatial dependence, the plane wave contributions from equation 1.1 and equation 1.3 needs to be incorporated.

When calculating Gaussian beam propagation through lenses and crystals it is possible to use the matrix formalism of geometric paraxial optics. With this it is not only possible to propagate beams through various optics; it is also possible to calculate what fundamental mode size a laser cavity will resonate in by an eigenvalue approach applied on the round trip matrix. This is a useful tool when designing a laser cavity.[15]

The Gaussian beam presented above is just the fundamental or lowest order Gaussian mode. Higher order modes exists both in cylindrical coordinates, in rectangular coordinates and in elliptical cylindrical coordinates. The elliptical coordinates are the continuous transition between the rectangular and the cylindrical coordinates.[21]

Hermite Gaussian (HG) modes are solutions of the paraxial wave equation in rectangular coordinates. Rectangular symmetry implies that the x and y coordinates can be decoupled. In a general high order HG mode the Gaussian field envelope is modulated by different Hermite polynomials and the resulting beam will consist of a set of lobes instead of the single lobe of the fundamental mode. The decoupling of x and y implied that the beam waist radius w_0 and position can be different in the x and y coordinate and the beam can thus be astigmatic in a an different way than the astigmatism given by the use of different Hermite polynomials in x and y. Higher order modes in cylindrical symmetry are called Laguerre Gaussian (LG) modes[22] and are modulated by Laguerre polynomials and the modes under elliptical symmetry are called Ince Gaussian (IG) modes and they are modulated by Ince polynomials.

All these forms complete sets, i.e. it is possible to decompose an arbitrary beam into a linear combination of HG, LG or IG modes. Thus it is also possible to describe a (higher order) mode in one set as a linear combination of modes of another set.[23,21] A property of a single Gaussian mode (lowest or higher order) is that the intensity distribution does not change with propagation. This is in stark contrast to the case of a general beam. As an example, consider a beam with a radially symmetric top hat intensity distribution in the near field. In the far field the radial intensity distribution will be that of an Airy pattern, with a set of weak rings surrounding a central lobe.

The fundamental Gaussian mode is the mode of least diffraction losses in a laser cavity as well as the mode with the best beam quality. One measure of the beam quality is the beam parameter product *BPP*, which is given by the product between the far field divergence angle θ and the waist size w_0.

$$BPP = \theta w_0 \tag{1.13}$$

In a lowest order Gaussian beam the product is λ/π, and for a general beam the value is higher. In a general beam the beam quality is often described by a single number, the M^2 number, which is independent of wavelength. The definition of M^2 is the quotient between the *BPP* of the beam and the *BPP* of a fundamental Gaussian beam.[24] For a lowest order Gaussian beam $M^2 = 1$, and for all other beams $M^2 > 1$.

The measurement of the *BPP* parameter requires a well defined beam size. The beam size description used for the fundamental Gaussian mode above will be of little value for the measurement of a general laser beam, since the structure of the intensity distribution can lead to ambiguities. There might very well be several radii where the intensity drops below the threshold value of e^{-2} times the on-axis value. Several other beam size definitions are used, including that of "power in a bucket" – i.e. the size needed to enclose a certain fraction (e.g. 86.5%) of the total beam power. The ISO standard ISO 11146[25] defines the beam sizes as a statistical quantity – w_0 is twice the standard deviation of the intensity or twice the square root of the variance or the second order moment. The beauty of this definition is that the propagation of an arbitrary beam can be described by the simple equations of 1.10, as long as λ is exchanged for $M^2\lambda$ in equation 1.9. In second order terms there is no difference[26] between

such a beam and a beam of wavelength $M^2\lambda$, though the actual beam intensity distribution can be very different, as the top hat beam example above shows.

A partially coherent beam can be characterized by its second order moments.[27,28] In the most general case the beam has ten independent second order moments, which gives information on the beam radii, far field divergences, radii of curvature, orientation of the beam in the near field and the far field, position of beam waists, etc. The propagation matrices of geometrical optics can be used to calculate the transformation of these properties as the beam propagates. A practical application of this is the symmetrization of an astigmatic beam to a symmetric beam, e.g. the output from a diode stack.[29]

1.5 Short pulses

Any laser with an intracavity element or process that favours high intensities will operate in pulsed mode. The generation of short laser pulses is divided into two different regimes, Q-switching and mode locking. In a Q-switched laser, the loss is high during most of the time, allowing energy storage in the active media. Then the loss is decreased substantially and the laser will start to lase. All the stored energy will feed an avalanche of photons, which decreases quickly again when the stored energy is drained. Thus a huge pulse is created. After the pulse is emitted, the loss is introduced again, allowing for the storage of energy for the next pulse. In a Q-switched laser the pulse lengths are longer than the cavity round trip time and the pulse repetition rate is lower than the inverse of the cavity round trip time. Every pulse is starting from spontaneous emission and the pulse to pulse variations in terms of energy can be significant. Since Q-switched laser pulses were not used in this work, no more will be written about them.

A mode-locked laser allows for much shorter pulses, down to a few cycles of the central frequency. In a mode-locked laser, there is a single pulse that oscillates back and forth and through the semi-transparent output coupler a pulse train is emitted. The mode-locked pulse is shorter than the cavity round trip time and the pulse repetition frequency is exactly the inverse of the cavity round trip time. More details on how the different cavity wavelengths interfere constructively to produce the short pulse are given in chapter 2.

In this brief part, the focus will be on the short pulses and how they propagate in dispersive media. The difference between the beam of a continuous laser and that of a pulsed laser is that the pulsed laser is not monochromatic and that, obviously, the field is modulated by a temporal envelope. In order to take dispersion into account the propagation constant k can be Taylor expanded around the central frequency. Here the treatment will be limited to stating the most important consequences of dispersion.

The two most well known and common temporal envelope functions of short laser pulses are the Gaussian (equation 1.14) and the hyperbolic secant (equation 1.15). A temporal envelope can be used together with spatial beam propagation such as the Gaussian beam results from the last section, provided that ω is replaced by the central frequency of the pulse ω_c, also known as the carrier frequency.

$$E_G(x,y,z,t) = \tilde{E}(x,y,z,t)\exp\left(-\left(\frac{z/v_g - t}{t_G}\right)^2\right) \tag{1.14}$$

$$E_S(x,y,z,t) = \tilde{E}(x,y,z,t)\,\mathrm{sech}\left(\frac{z/v_g - t}{t_S}\right) \tag{1.15}$$

Here the v_g is the group velocity defined by equation 1.16. The group velocity is the speed by which the pulse envelope moves and is equal to the speed of light in vacuum, c, divided by the group refractive index n_g.

$$v_g = \left[\left. \frac{dk}{d\omega} \right|_{\omega_c} \right]^{-1} = \frac{c}{n(\omega_c) + \omega \left. \frac{dn}{d\omega} \right|_{\omega_c}} = \frac{c}{n_g} \qquad 1.16$$

Two pulses of different polarizations or wavelengths that enter a crystal will separate from each other as they travel in the media. This is a consequence of different group velocities and the phenomenon is known as group velocity mismatch (GVM) and is of great importance when short pulses are used in frequency conversion schemes. Furthermore, different spectral components will travel with different group velocity in a pulse and as a result the pulse broadens with distance in the dispersive media. This is known as group velocity dispersion (GVD) and is characterized by the dispersion length L_D.

A common quality measure for mode locked pulses is the time bandwidth product (*TBP*). This is the product of the pulse length t_p or Δt and the frequency spectrum Δv, both measured in the full width half max (FWHM) sense. If a pulse with a certain pulse shape has the *TBP* of the corresponding entry in table 1.1, then the pulse is said to be transform limited. If the valued of Δt and Δv are measured in the root-mean square sense, the Gaussian pulse will have a *TBP* of $(4\pi)^{-1}$, and any other pulse shape will have a larger value. There is an analogy between the dispersion of a Gaussian pulse and the diffraction of the Gaussian fundamental spatial mode with temporal equivalents of equations 1.7-1.10.[30]

	TBP	$\Delta t = t_p$
Gaussian	0.4413	$t_G \cdot 2\sqrt{ln\,2}$
Hyperbolic secant	0.3148	$t_S \cdot 2\,ln\left(1+\sqrt{2}\right)$

Table 1.1 Time bandwidth products for Gaussian and hyperbolic secant pulses. The relations between the FWHM pulse length and the function-related times t_G and t_S are also provided.

Chapter 1

Chapter 2

Mode-Locked Lasers

2.1 Photons and matter

Three of the fundamental ways by which photons and matter interact are spontaneous emission, absorption and stimulated emission.[14] Consider the case of an atom (or a molecule) with two energy levels, 1 and 2, of energies E_2 and E_1 ($E_2 > E_1$). The energy gap corresponds to a photon of angular frequency ω, as defined in equation 2.1, where h is Planck's constant.

$$\omega = \frac{2\pi(E_2 - E_1)}{h} \qquad 2.1$$

- Spontaneous emission. The atom decays from the upper level to the lower level though the emission of a photon of angular frequency ω. The emitted photon has a random phase and a random direction and the time is random too, obeying Poisson statistics.
- Absorption. The atom, being in level 1, absorbs an incident photon and is raised to level 2.
- Stimulated emission. If the atom is in level 2, and a photon of angular frequency ω passes by, then the atom is stimulated to emit a photon of the same frequency. Furthermore, the two photons will be in phase with each other and they will travel in the same direction. The stimulated photon thus inherits the properties of the stimulating photon.

The three processes are depicted in figure 2.1.

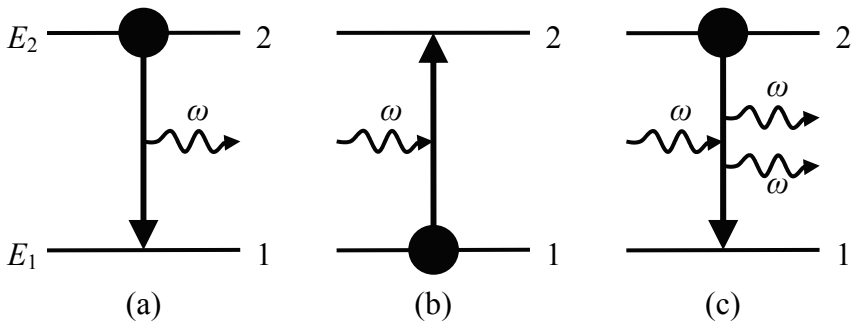

Figure 2.1 (a) Spontaneous emission. (b) Absorption. (c) Stimulated emission.

For the more interesting case of an ensemble of active atoms we introduce the population density N_i, being the number of atoms per unit volume in the level i. The degeneracy of level i is given by the degeneracy factor g_i, but in the following the levels will be assumed to be nondegenerate, i.e. $g_i = 1$ for all i. The treatment can be made more general by the substitution from N_i to N_i / g_i.

In thermal equilibrium the ratio between N_2 and N_1 is given by Boltzmann statistics, where k_B is the Boltzmann constant and T is the temperature in Kelvin:

$$\frac{N_2}{N_1} = exp\left(-\frac{E_2 - E_1}{k_B T}\right) \qquad 2.2$$

Thus there will be more atoms in level 1 than in level 2 under thermal equilibrium. The rate of created photons will be proportional to the photon flux and the density of atoms in level 2. In the same way the rate of lost photons is proportional to the photon flux and the density of atoms in level 1. Einstein showed in 1917 that the proportionality factor for absorption and stimulated emission are equal[31] and therefore the requirement of optical gain is that there is a population inversion, i.e. that $N_2 > N_1$.

2.2 Ideal four-level laser

It is not possible to achieve steady state population inversion in a two level system, since the system becomes transparent at $N_2 = N_1$. The easiest way to reach population inversion is to use a four level scheme. Most atoms are in the ground state, level 0. A pump process transfers them to a broad pump level, level 3. From there the system decays to the upper laser level, level 2. The decay is a rapid non-radiative process. The upper laser level should have a long life time, so that it is easy to populate. The lower laser level, level 1, is virtually empty since a rapid decay transfers the atoms back to the ground state. Thus population inversion is created by a minimum of pump. In the simplest model, every atom that is transferred into the pump level will transfer to the upper laser level, where stimulated emission occurs. The system described above is depicted in figure 2.2.

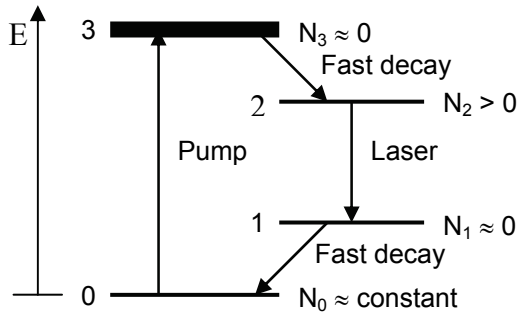

Figure 2.2. Four-level laser scheme. Pump photons transfer atoms from the ground state (0) to the broad pump band (3). Lasing takes place between the upper (2) and the lower (1) laser level when the population density $N_2 > N_1$. Fast decays depopulate the pump level and the lower laser level.

There is a multitude of rate equations describing the rates of change in the population densities as well as in the photon flux. The complexity varies from the idealized scheme above to schemes incorporating more energy levels and detrimental parasitic processes as well as geometric factors and heating effects. Rate equations is a useful tool in modelling laser cavities, both for the steady state (continuous wave) regime and in the dynamic regime.[32,33]

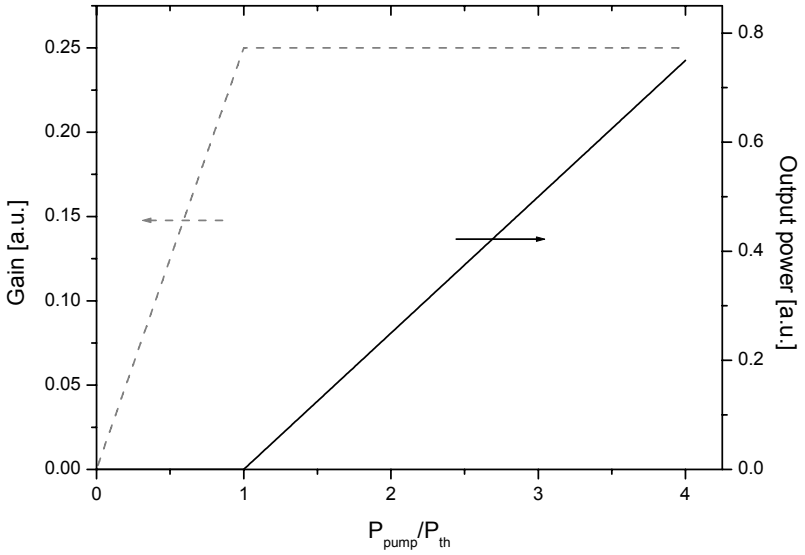

Figure 2.3. The input-output characteristics of an ideal four level laser.

Population inversion is a necessary condition for lasing action, but it is not sufficient. There will be losses for the light travelling in the cavity and in order to achieve lasing the gain must equal the loss. The pump power needed for the gain to equal the loss is called the threshold power and when threshold is reached the gain is clamped to the loss value and lasing begins. As the pump power is increased, so will the output power. In the ideal four level laser, as in most real lasers, the growth is linear, characterized by the slope efficiency. This is illustrated in figure 2.3.

Other laser schemes include the three level lasers, where the lower laser level is the ground state of the system. The condition for population inversion is then that half of the population in the ground state is raised to the upper laser level, which means that a very efficient pump scheme is required. The threshold power of such lasers is high. The lower laser level can be a sublevel of the ground state, with a significant population density at room temperature. These lasers are called quasi three level lasers and they also require efficient pump schemes and sources due to the inherently high pump threshold.

2.2.1 Nd doped laser crystals

Neodymium doped Yttrium Orthovanadate (Nd:YVO_4) is YVO_4 crystal where a small percentage of the Y^{3+} ions are replaced by the active laser ion Nd^{3+}. Typical dopant levels are between 0.3 atomic % and 3 atomic %. The material has good optical and mechanical properties and is one of the most efficient laser crystals for diode pumping, with optical to optical efficiencies of 68% demonstrated.[34] This is because it has a broad, smooth and strong absorption peak around 808 nm, where high quality pump lasers are available and because the stimulated emission cross section is large at the main four-level lasing wavelength of 1064 nm. The crystal is uniaxial and hence birefringent and most properties differ between the crystal c axis and the plane perpendicular to it. The output of an Nd:YVO_4 laser is intrinsically linearly polarized, which is convenient when the light is to be used in nonlinear optical experiments.

$GdVO_4$ is an isomorph of YVO_4, with gadolinium ions replacing the yttrium ions. The materials have very similar properties the most notable difference being that the laser

wavelength of Nd:$GdVO_4$ is slightly lower with a peak at 1063 nm. Both crystals are well suited for proof-of-principle experiments.

2.3 Mode locking

In a laser there are normally several longitudinal modes. When they oscillate with a common phase, then the different wavelengths will interfere constructively to create a single pulse, oscillating back and forth in the cavity and at the output coupler a pulse train will be emitted.

The wavelengths supported by a laser cavity are those that fulfil the standing wave condition of fitting an integer number of half wave lengths between the end mirrors. The angular frequency ω_q of the q^{th} longitudinal cavity mode is given by equation 2.3 and the mode spacing is thus given by equation 2.4:

$$\omega_q = q\frac{\pi c}{L'} \tag{2.3}$$

$$\Delta\omega = \frac{\pi c}{L'} \tag{2.4}$$

L' is the optical length of the cavity. In general, the mode in a laser cavity will be a fundamental Gaussian mode and the cavity frequencies will be slightly different due to the Gouy phase shift. The field will then be modified, but for this treatment plane waves is adequate. Consider a cavity with N longitudinal modes. The angular frequency of the first mode is ω_1 and ω_m is then given by equation 2.5. The total field is the sum of the individual fields and in the most general case both the fields E_m and the phase φ_m can be different.

$$\omega_m = \omega_1 + (m-1)\Delta\omega \tag{2.5}$$

$$E(z,t) = \tfrac{1}{2}\sum_{m=1}^{N} E_m \exp\left(i\omega_m(z/c - t) - i\varphi_m\right) + c.c \tag{2.6}$$

In a continuous wave laser, the phases are random and the intensity distribution is random too. There will be intensity fluctuations and spikes with a temporal width corresponding roughly to the inverse of the spectral bandwidth. The temporal behaviour when modes have a common phase, φ_0 is that of a single strong pulse.[35] For simplicity it is assumed that all the modes have a common amplitude E_0.

$$\begin{aligned} E(z,t) &= \tfrac{1}{2}\sum_{m=1}^{N} E_0 \exp\left(i\omega_m(z/c - t) - i\varphi_0\right) + c.c. \\ &= \tfrac{1}{2} E_0 \exp\left(i\frac{\omega_1 + \omega_N}{2}(z/c - t) - i\varphi_0\right)\frac{\sin\left(N\Delta\omega(z/c - t)\right)}{\sin\left(\Delta\omega(z/c - t)\right)} + c.c. \end{aligned} \tag{2.7}$$

The final expression has two parts, a plane wave and a modulation term. The angular frequency of the plane wave is just the average of those of the included modes, i.e. the carrier frequency. The modulation function sin(Nx)/sin(x) has a large peak when x is a multiple of π – this corresponds to an interval of 2L' for z and thus there is only one pulse in the cavity. There are also smaller intermediate peaks in between the huge peaks. In a real laser the amplitude of the different modes will not be equal. The distribution will be bell shaped, e.g.

Gaussian, and the output will lack the small intermediate peaks. Thus there will be a single, bell-shaped pulse in the cavity.

2.3.1 Mode locking schemes

Mode locking can be achieved both by active and by passive means. In an actively mode locked scheme the mode locking element is driven by an external source. The pulse lengths available are limited by the modulation provided and in general active mode locking techniques generate longer pulses than passive techniques. The external source adds complexity to the laser, but on the other hand allows for synchronization with other equipment. Passive mode locking hinges on a nonlinear optical effect, such as saturation in a saturable absorber or the intensity dependent refractive index in a suitable material.

Active mode locking schemes employ intracavity modulators to force the normally independent longitudinal cavity modes to oscillate in phase and thereby produce trains of short pulses. The modulators are based on amplitude or phase modulation and the period of the modulation is equal to the cavity round trip time. Mode locking can be analysed in the frequency domain or in the time domain. The time domain picture can seem more intuitive and will be used in the following paragraphs. The frequency domain picture of active mode locking is based on the observation that by modulating the cavity field at the right frequency, every longitudinal mode will create sidebands corresponding to neighbouring modes and thus all cavity modes will be coupled.[14]

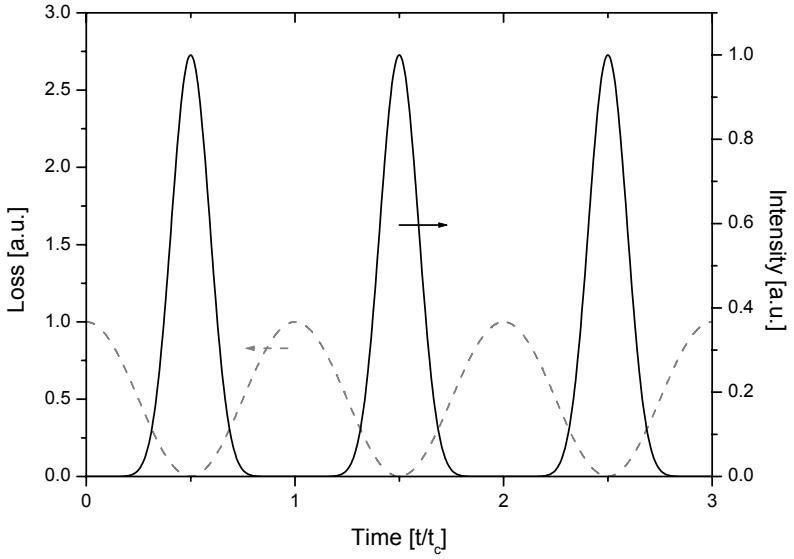

Figure 2.4. Active mode locking by amplitude modulation. A loss modulation at the cavity repetition frequency $1/t_c$ supports pulses that pass the modulator at when the loss is at a minimum.

The periodic loss modulation of amplitude modulated active lasers can be realized by several different means. Most commonly the intracavity element is an acousto-optical modulator[10] or an electro-optical modulator.[36] The mode locking operation is easy to understand in the time domain, since a pulse passing the loss modulation at the moment of maximum transmission is clearly favoured. The pulse shortening mechanism is provided by the fact that the loss is higher for the leading and the trailing edge of the pulse. These are thus suppressed and the resulting pulse is shorter. See figure 2.4 for an illustration. The shorter the pulse becomes compared to the modulator period, the less efficient is the pulse shortening

process. The pulse shortening is counteracted by a pulse broadening arising from the finite gain bandwidth.

Phase modulation is most commonly provided by an electro-optical modulator,[37] but other equivalent options including that of a piezo-electric oscillating end mirror[38] are also possible. A phase modulator with a period tuned to the cavity round trip time will also favour short pulses, a fact that is easiest explained in terms of an oscillating mirror. A pulse that is reflected at the mirror when it is moving will do so every time is passes by, and the accumulated Doppler shift will move the frequency out of the gain region of the active media. Light that is reflected by the mirror when it is at one of the two end positions will not experience any Doppler shift and can thus be amplified. The two end positions implies two possible oscillating pulses (see figure 2.5) and lasers mode locked by pure phase modulation tend to switch between the two. Another downside of phase modulation is that the pulses will acquire a parabolic phase variation and this chirp results in longer pulses than those generated by amplitude modulation of the same frequency bandwidth.[14] The advantages of phase modulation are simplicity and low insertion losses.

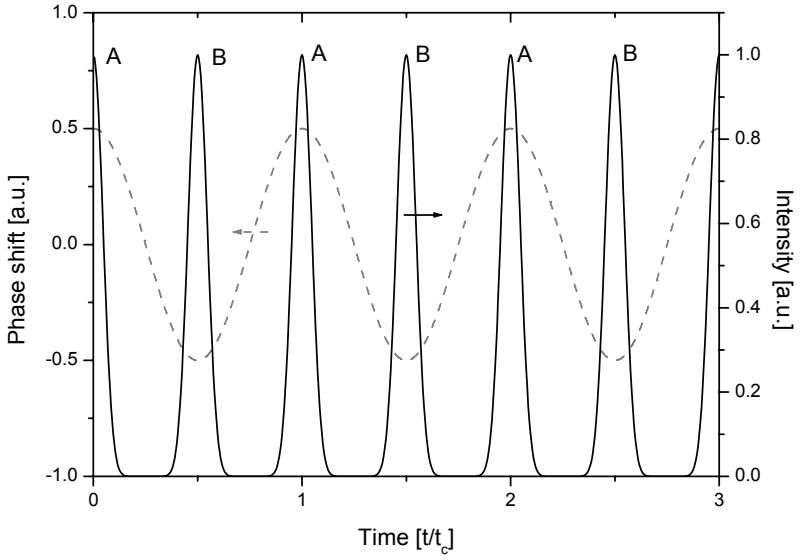

Figure 2.5. Active mode locking by phase modulation. There are two possible solutions, A and B, corresponding to the turning points of the phase modulation.

Among the passive schemes the classical method is the fast saturable absorber (SA). A dye or a semiconductor with an upper state life time that is short compared to the cavity round trip time is used. A fast saturable absorber favours high intensities in the following way: low intensity light is absorbed by the SA, but when a short pulse passes by, the absorber is bleached or saturated by the leading edge of the pulse and the central part can pass the SA with very small absorption losses. If the laser is well designed, gain saturation will cause pulse shortening in the trailing edge of the pulse too. The pulse lengths were further reduced by the colliding pulse mode locking technique,[39] where two counter-propagating pulses in a ring cavity meet at the saturable absorber. Saturable absorbers are used for passive Q-switching too, and it was in that context that the first pulses mode locked by dyes were observed[40,41] in the mid 60's. The semi-conductor equivalent[42] came later and has in the form of the semiconductor saturable absorber mirror (SESAM) been very successful.[43] Saturable absorbers with recovery times in the order of the cavity round trip time can under special circumstances be used to mode lock lasers.[44] These are known as slow saturable absorbers.

A completely different scheme is that of coupled cavity mode locking,[45] also known as additive pulse mode locking. In this scheme a second cavity of equal optical length is added to the first and inside this extra cavity there is a nonlinear element, typically an optical fibre exhibiting an intensity dependent refractive index, $n = n_0 + n_2 I$. The added cavity is then a Fabry-Perot resonator where the reflectivity is intensity dependent and a correctly adjusted cavity length will favour mode locked pulses. This scheme, in contrast to the other passive schemes, requires interferometric control of the cavity lengths.
The passive mode locking technique that has produced the shortest pulses[46,47] is Kerr lens mode locking (KLM).[48] In order to achieve pulses with only a few optical cycles the cavity net dispersion must controlled. The positive dispersion of optical elements such as the active media must be counteracted by the insertion of cavity elements with negative net dispersion, such as dispersive mirrors[49] or the prism combination demonstrated by Fork *et al*.[50] KLM is based on the third order nonlinear effect of intensity dependent refractive index in combination with an intracavity soft or hard aperture. A laser beam propagating in a media with a nonlinear refractive index, $n = n_0 + n_2 I$, will acquire an additional phase due to the nonlinear refractive index variation. Since a Gaussian beam has an intensity distribution that can be approximated by a parabola around the centre, the added phase is parabolic and the media thus acts as a nonlinear lens. This spatial effect is known as Kerr lensing. The focusing effect depends on the intensity and if the media is combined with a correctly placed intracavity aperture the process will favour high intensities and mode locking will occur. The principle of KLM is illustrated in figure 2.6. The temporal intensity variation of a mode locked intracavity pulse will cause pulse shortening since the aperture removes low intensity fields.

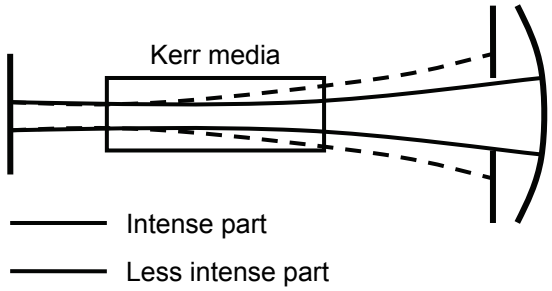

Figure 2.6. Illustration of Kerr lens mode locking. The intense parts of the field will be focussed more and experience less diffraction losses at the aperture.

There are three distinct mode locking techniques based on cascaded second order nonlinearities, typically second harmonic generation followed by difference frequency generation. A limited theory of cascaded interactions is found in chapter 4. In this context it is sufficient to say that the methods based on cascading involves the conversion of fundamental wave light into the second harmonic followed by back conversion. The nonlinear mirror mode locking technique[51] employs a dichroic mirror with larger reflectivity for the second harmonic light than for the fundamental light. The mirror is positioned between the cascaded processes and since the second harmonic generation efficiency depends on intensity the mirror reflectivity of the fundamental will increase with intensity,[52] thus favouring short pulses. The nonlinear polarisation evolution or quadratic polarization switching technique[53] utilises an intensity dependent polarisation rotation,[54,55] typically produced by the complete conversion and back conversion of one polarisation component in an unbalanced type II second harmonic generation process, though it can be produced in type I interactions as well.[56] The third technique, called cascaded second order nonlinearity mode locking[57] or more informatively

cascaded Kerr lens mode locking [I] is based on the fact that the cascading of second harmonic generation and difference frequency generation can emulate the third order Kerr effect.[58] A basic theory for the cascaded Kerr effect is provided in chapter 4, together with the descriptions of two experimental realizations of the concept [I,II].

Chapter 3

Fundamental Aspects of Nonlinear Optics

The field of nonlinear optics can be divided into two parts, resonant and non-resonant nonlinear optics. When pumping a system at resonance the nonlinear response is very strong and thus the effects can be studied even with light sources of moderate intensity. This field was active before the first lasers came along. In the following, the description of nonlinear optics will be limited to non-resonant processes.

The birth of modern nonlinear optics came with the second harmonic generation experiment by Franken *et al.*[12] in 1961, just one year after the invention of the laser. Frequency conversion processes were well-known in other parts of the electromagnetic spectrum but before the laser was invented there was no means of achieving the high intensities needed for e.g. second harmonic generation in the optical regime. Since 1961 the field have grown tremendously and new processes and phenomena have been discovered.

In the description of non-resonant nonlinear interactions a very practical and useful approach is to treat the nonlinearity as a small perturbation. This is the treatment used in this thesis. It should also be stated that this approach does not cover the case of extremely intense fields, when the nonlinear response simply becomes too strong to be treated as a perturbation. The theory presented here is by necessity very limited. For more detailed treatments there are textbooks available.[59,60,61,62]

3.1 Maxwell's equations

The way light and matter interact can be seen to have two parts - the electromagnetic wave induces a response in a medium and the medium in reacting modifies the field. The first part is governed by the constitutive equations and the latter by the Maxwell's equations.[59]

Maxwell's equations (equations 3.1-4) governs the time and space evolutions of the electric field $\boldsymbol{E}$ and magnetic field $\boldsymbol{H}$, taking into account the free current density $\boldsymbol{J}$ and free charge densities ρ of the media where the interaction takes place.

$$\nabla \cdot \boldsymbol{D} = \rho \tag{3.1}$$

$$\nabla \cdot \boldsymbol{B} = 0 \tag{3.2}$$

$$\nabla \times \boldsymbol{E} = -\frac{\partial \boldsymbol{B}}{\partial t} \tag{3.3}$$

$$\nabla \times \boldsymbol{H} = \boldsymbol{J} + \frac{\partial \boldsymbol{D}}{\partial t} \tag{3.4}$$

In the equations above the displacement field $\boldsymbol{D}$ and the magnetic flux density $\boldsymbol{B}$ are also present. These quantities shows the influence of the media and are related to the other fields by the constitutive relations.

The constitutive relations (equations 3.5-7) deal with how the fields affect the polarization $\boldsymbol{P}$, the magnetization $\boldsymbol{M}$ and the current and charge densities. Often the law of charge conservation (equation 3.8) is included with the constitutive relations.

$$\boldsymbol{D} = \varepsilon_0 \boldsymbol{E} + \boldsymbol{P} \tag{3.5}$$

$$\boldsymbol{B} = \mu_0 \left(\boldsymbol{H} + \boldsymbol{M} \right) \tag{3.6}$$

$$\boldsymbol{J} = \sigma \boldsymbol{E} \tag{3.7}$$

$$\nabla \cdot \boldsymbol{J} + \frac{\partial \rho}{\partial t} = 0 \tag{3.8}$$

Here μ_0 is the magnetic permeability of free space and σ is the conductivity of the material. In the general case all these are entities are nonzero. Knowing Maxwell's equation and applying the correct boundary conditions as well as the correct constitutive relations it is in principle possible to solve the time and space evolution of any electromagnetic field. In general this is mathematically tricky and in general physically motivated approximations are needed. For instance the response of metals is mainly governed by the free charges and in magnetic materials the magnetization is nonzero. In semiconducting materials both the free charge density and the polarization is important. In our case there are some simplifications that can be applied. The media we use are dielectrics, which means that there are no free charges ($\rho = 0$), no associated free currents ($\boldsymbol{J} = 0$), no magnetization ($\boldsymbol{M} = 0$) and the polarization $\boldsymbol{P}$ is thus the sole link between the fields and the material.

3.2 The nonlinear response of dielectric media

Dielectric media, such as glass, water and the crystals used in the experiments presented in this thesis can be seen as positively charged atom cores surrounded by electron clouds. When a dielectric media is subjected to an electric field $\boldsymbol{E}$, the charge density distribution of the electrons changes and a dipole moment is created. Due to their larger weight, the atom cores are in principle immobile. The dipole moment per unit volume is called polarization and is denoted $\boldsymbol{P}$. As long as the field is weak, the polarization is directly proportional to the field.

$$\boldsymbol{P} = \boldsymbol{P}^L = \varepsilon_0 \boldsymbol{\chi}^{(1)} \boldsymbol{E} \tag{3.9}$$

Here the linear polarization is denoted $\boldsymbol{P}^L$, ε_0 is the permittivity of vacuum and $\boldsymbol{\chi}^{(1)}$ is the first order susceptibility tensor. If the electric field is part of an electromagnetic wave, e.g. light, then the induced polarisation consists of oscillating dipoles. These will radiate and the field is modified by this contribution. Depending on the strength, phase and direction of the contribution, the media will have different material properties in terms of refractive index and absorption. All this is incorporated in the complex linear susceptibility tensor. The refractive index n is given by equation 3.10 and if the media is lossless then the tensor is real-valued. For simplicity the tensor is replaced by a constant.

$$n = \sqrt{\mathrm{Re}\left(1 + \chi^{(1)}\right)} \tag{3.10}$$

Within the linear regime all concepts of classical optics can be explained, such as refraction, reflection, polarization, diffraction, interference, absorption etc.

When the field is strong, the electron cloud displacement is large enough so that adjacent atoms will influence and the response is no longer linear.[63] The nonlinear response $\boldsymbol{P}^{NL}$ is then described by a power series expansion of the polarization.

$$\boldsymbol{P} = \boldsymbol{P}^{L} + \boldsymbol{P}^{NL} = \varepsilon_0 \boldsymbol{\chi}^{(1)} \boldsymbol{E} + \varepsilon_0 \left(\boldsymbol{\chi}^{(2)} \boldsymbol{E}^2 + \boldsymbol{\chi}^{(3)} \boldsymbol{E}^3 + \ldots \right) \qquad 3.11$$

The susceptibility tensors $\boldsymbol{\chi}^{(m)}$ are of rank (m+1) and they are rapidly decreasing in magnitude with increasing power m. In this thesis the focus will be on second order interactions.

3.3 Second and third order processes

A nonlinear process normally involves a flow of energy from one or several optical fields into a set of new fields. The processes are reversible, but then they are named differently, as will be seen in the following.

The second order polarisation is the strongest and gives rise to several practical and interesting effects. In the general case involving quasi-monochromatic light, the polarization is created from two electrical fields $\boldsymbol{P}^{(2)} = \varepsilon_0 \boldsymbol{\chi}^{(2)} \boldsymbol{E}_1 \boldsymbol{E}_2$, which may be degenerate. One of the fields can be a slowly varying or a static electric field, as in the case of the linear electro-optic (or Pockels) effect. This modifies the refractive index and is widely used in optical modulators. The effect can work backwards, too, when a static field is crated from a degenerate optical field in the process of optical rectification (OR).

The second order frequency converting processes can be divided into two groups, one for generating an energetic photon out of two low-energy photons and one group for splitting a photon into two photons of lower energy.

The most well-known second order nonlinear process is that of second harmonic generation (SHG). Here two identical photons are converted into a single photon of double energy. This is the degenerate version of the nondegenerate process of sum frequency generation (SFG), where the energetic photon is created from two different input photons.

The opposite process of SFG is difference frequency generation (DFG), where an energetic photon is split into two photons of less energy. This splitting is stimulated by the presence of one of the low energy photons and the process is also known under the name of optical parametric amplification (OPA).

The photon splitting can also take place seeded with quantum noise and then it is called optical parametric generation (OPG). The same process is known under the name of optical parametric oscillation (OPO), when the crystal is placed between mirrors resonating one or several fields.

Among the many third order processes possible only one is relevant for this work, namely the intensity dependent refractive index (IDRI), described by a nonlinear index of refraction, $n = n_0 + n_2 I$. The variation of the refractive index obviously has no meaning unless the intensity varies too. Spatial variation of the intensity, as is the case in a Gaussian beam, leads to the optical Kerr effect, more informatively known as Kerr lensing. Temporal variation of intensity, as in the case of short pulses, leads to self phase modulation where the pulse is chirped. IDRI can also be achieved by the cascading of SHG and DFG. This is described in chapter 4 and used in the experimental work [I, II].

3.4 Symmetry considerations

When the frequencies involved in the fields of equations 3.9 and 3.11 are smaller than the lowest resonance frequency of the material then the response is essentially instantaneous. This

is the case for the optical frequencies in the non-resonant description here and it validates the equations with $\boldsymbol{E}$ and $\boldsymbol{P}$ as time-dependent quantities as implicitly understood in the description above.[62] When using laser light it is more convenient to work in the frequency domain, since the electric field and the nonlinear polarization can be thought of as a superposition of different monochromatic frequency components. This allows us to take the Fourier transforms of the fields and the susceptibilities. In equation 3.12 there is an example of a second order relation in the frequency domain.

$$P_i^{(2)}(\omega_3) = \varepsilon_0 \chi_{ijk}^{(2)}(-\omega_3; \omega_1, \omega_2) E_j(\omega_1) E_k(\omega_2) \qquad 3.12$$

A polarization of angular frequency ω_3 is generated at the Cartesian coordinate i by the tensor element connecting the electric fields of frequencies ω_1 and ω_2 at the Cartesian coordinates j and k, respectively. In the notation for the tensor element a minus sign indicates a generated frequency. The relation between the frequencies is fixed by the energy conservation requirement of equation 3.13:

$$-\omega_3 + \omega_1 + \omega_2 = 0 \qquad 3.13$$

In the most general case, there are different χ elements for all combinations of frequencies and Cartesian coordinates. The order of the electric fields does not matter though, as long as the coordinates is permutated as well. This is the intrinsic permutation symmetry.

If the media is lossless for all frequencies involved in equation 3.12 then all the frequencies including the polarization frequency can be permutated together with the corresponding Cartesian coordinates. Not only that, but the signs of the frequencies can be changed as long as equation 3.12 is valid and the generated polarization frequency carries a negative sign. This means that different physical processes will have the same nonlinear coupling, e.g. the tensor element for sum frequency generation will be the same as that of optical parametric generation.[61] In the stricter case of Kleinman symmetry, i.e. when there is no material resonances close to or in between any of the interacting frequencies, then the frequencies can be permutated freely without changing the Cartesian coordinates.

In the general case crystals are optically anisotropic, i.e. optical properties as the refractive index, absorption coefficient and nonlinearity varies depending on the polarization and the direction of the light. In the perturbation approach this is dealt with by the fact that the electric susceptibility of order m is a tensor of rank (m+1).

Depending on the crystal structure and on the symmetry relations that can be used the number of non-zero and independent tensor entries can vary a lot. In particular, for crystals that have a centre of symmetry all even orders of the susceptibility tensors will be zero. This is also the case for isotropic material, e.g. glass. Other crystal symmetries, such as mirror plane or rotation axis symmetries will also cause some tensor elements to be zero or ±1 times other elements. Under Kleinman symmetry the number of independent and non-zero elements will be further reduced.

The use of tensors can be cumbersome and in the case of the second order interactions it is common to use a d-coefficient formalism. This reduces the number of independent elements from 27 to 18 and is valid due to the intrinsic permutation symmetry for the case of second harmonic generation but can be extended to all second order processes under Kleinman symmetry. In the strict non-dispersive limit of Kleinman symmetry, there are 10 independent elements at most.[64] The relation between $d^{(2)}$ and $\chi^{(2)}$ is given by equations 3.14 and 3.15 and in equation 3.16 the second order polarization is given in the d-coefficient notation.

$$d_{ij}^{(2)} = \frac{1}{2}\chi_{ikl}^{(2)} \tag{3.14}$$

$$\begin{array}{lcccccc} j: & 1 & 2 & 3 & 4 & 5 & 6 \\ kl: & 11 & 22 & 33 & 23, 32 & 13, 31 & 12, 21 \end{array} \tag{3.15}$$

$$\begin{bmatrix} \left(P_{\omega_3}^{(2)}\right)_x \\ \left(P_{\omega_3}^{(2)}\right)_y \\ \left(P_{\omega_3}^{(2)}\right)_z \end{bmatrix} = 2\varepsilon_0 K \begin{bmatrix} d_{11} & d_{12} & d_{13} & d_{14} & d_{15} & d_{16} \\ d_{21} & d_{22} & d_{23} & d_{24} & d_{25} & d_{26} \\ d_{31} & d_{32} & d_{33} & d_{34} & d_{35} & d_{36} \end{bmatrix} \begin{bmatrix} \left(E_{\omega_1}\right)_x\left(E_{\omega_2}\right)_x \\ \left(E_{\omega_1}\right)_y\left(E_{\omega_2}\right)_y \\ \left(E_{\omega_1}\right)_z\left(E_{\omega_2}\right)_z \\ \left(E_{\omega_1}\right)_y\left(E_{\omega_2}\right)_z + \left(E_{\omega_1}\right)_z\left(E_{\omega_2}\right)_y \\ \left(E_{\omega_1}\right)_x\left(E_{\omega_2}\right)_z + \left(E_{\omega_1}\right)_z\left(E_{\omega_2}\right)_x \\ \left(E_{\omega_1}\right)_x\left(E_{\omega_2}\right)_y + \left(E_{\omega_1}\right)_y\left(E_{\omega_2}\right)_x \end{bmatrix} \tag{3.16}$$

Here $K(-\omega_3;\ \omega_1,\ \omega_2)$ is a degeneracy factor which has the value of $K = ½$ for the indistinguishable fields involved in SHG and optical rectification and $K = 1$ for all the other conversion processes. The convention of using *d*-coefficients will be used in the rest of this treatment.

The tensor algebra can be avoided completely by using the convention of the effective *d*-coefficient, d_{eff}. This form reduces the summation over several tensor elements in 3.16 to the compact, simple scalar relation of equation 3.17. The expressions for d_{eff} are simply the weighted combinations of the relevant tensor elements, where the weights come from the directional cosines of the polarizations of the interacting fields. In short, trigonometric relations based on the crystal structure, geometry and involved polarizations.[65,66]

$$P^{(2)}(\omega_3) = d_{eff} E_1(\omega_1) E_2(\omega_2) \tag{3.17}$$

The equation facilitates scalar wave equations, which are used to calculate how the generated fields will depend on interaction length and the intensities of the interacting fields.

3.5 The coupled wave equations

In order to predict the evolution and interaction of the different electromagnetic waves in a nonlinear process Maxwell's equations must be used. For a dielectric media they can be simplified to equations 3.18-21 by applying the simplifications of $\boldsymbol{M} = 0$, $\boldsymbol{J} = 0$, $\sigma = 0$ and $\rho = 0$ and using equations 3.5-6:

$$\varepsilon_0 \nabla \cdot \boldsymbol{E} + \nabla \cdot \boldsymbol{P} = 0 \tag{3.18}$$

$$\nabla \cdot \boldsymbol{H} = 0 \tag{3.19}$$

$$\nabla \times \boldsymbol{E} = -\mu_0 \frac{\partial \boldsymbol{H}}{\partial t} \tag{3.20}$$

$$\nabla \times \boldsymbol{H} = \varepsilon_0 \frac{\partial \boldsymbol{E}}{\partial t} + \frac{\partial \boldsymbol{P}}{\partial t} \tag{3.21}$$

Applying the curl operator to equation 3.20 and eliminating the magnetic field by the help of equation 3.21 leads to the general polarization driven vectorial wave equation, valid for both linear and nonlinear optics:[60]

$$\nabla \times \left(\nabla \times \tilde{\boldsymbol{E}}\right) = -\varepsilon_0 \mu_0 \frac{\partial^2 \tilde{\boldsymbol{E}}}{\partial t^2} - \mu_0 \frac{\partial^2 \tilde{\boldsymbol{P}}}{\partial t^2} \tag{3.22}$$

Here and in the following the tilde sign stands for a rapidly varying field. This can be further simplified in the case of quasi-cw infinite plane waves travelling along a principal axis, x, of the crystal. The direct consequence is that the energy flux is in the same direction as the wave vector and the following simplification can be used:

$$\nabla \times \nabla \times \tilde{\boldsymbol{E}} \approx -\nabla^2 \tilde{\boldsymbol{E}} \approx \frac{\partial^2 \tilde{E}}{\partial x^2} \tag{3.23}$$

The infinite plane wave approximation is not physical, but as long as the transverse variation is slow on the scale of a wavelength is a good approximation, and one well worth doing, since a lot of basic nonlinear optics can be explained in this framework. There are cases when the plane wave approximation breaks down, but in many cases the plane wave results can be modified slightly to incorporate the effects of focussing, Gaussian beam profiles, beam walk-off, short pulses etc., as has been done in sections 4.5 and 4.6.

The total field are a superposition of contributions of different frequencies and as well as being valid for the total fields, the wave equation is by necessity valid for each frequency component. In the following I will derive the spatial evolution of a field at angular frequency ω driven by the nonlinear polarization. So, both the electromagnetic waves and polarizations are of the form:

$$\tilde{E}_\omega(x,t) = \frac{1}{2}\left[E_\omega(x,t) exp\left[i\left(k_\omega x - \omega t\right)\right] + c.c.\right] \tag{3.24}$$

$$\tilde{P}_\omega^{NL}(x,t) = \frac{1}{2}\left[P_\omega^{NL}(x,t) exp\left[i\left(k_\omega' x - \omega t\right)\right] + c.c.\right] \tag{3.25}$$

Here and in the following the subscript ω associates the parameters with the angular frequency ω. $E_\omega(x,t)$ is the amplitude of the electric field envelope and k_ω is the wave vector. It should be noted here that the wave vector of the electric field k_ω need not be equal to that of the polarization, marked by a prime. This is because the polarization is in general driven by electromagnetic waves at other frequencies and thus at other phase velocities.

$$k_\omega = \frac{n_\omega \omega}{c} \tag{3.26}$$

The refractive index is given by n_ω and c is the speed of light in vacuum.

In all cases apart from the ones of very short pulses the slowly varying envelope approximation (SVEA) is valid. In means that the phase and amplitude of the field envelopes

is varying very slowly over the distance of a wavelength (equation 2.26) and over the time of a period (equations 2.27-28). In the following the *x* and *t* arguments are suppressed in the amplitude parameters.

$$\left|\frac{\partial^2 E_\omega}{\partial x^2}\right| << \left|k\frac{\partial E_\omega}{\partial x}\right| \tag{3.27}$$

$$\left|\frac{\partial^2 P_\omega}{\partial t^2}\right| << \left|\omega\frac{\partial P_\omega}{\partial t}\right| << \left|\omega^2 P_\omega\right| \tag{3.28}$$

$$\left|\frac{\partial^2 E_\omega}{\partial t^2}\right| << \left|\omega\frac{\partial E_\omega}{\partial t}\right| << \left|\omega^2 E_\omega\right| \tag{3.29}$$

So, starting at the vectorial wave equation 2.21, applying the plane wave result of 2.22, invoking the temporal SVEA 2.27 and 2.28 and applying equations 2.10 and 2.25 we arrive at

$$\frac{\partial^2 \widetilde{E}}{\partial x^2} + \varepsilon_0\mu_0\left(1+\chi^{(1)}\right)\frac{\partial^2 \widetilde{E}}{\partial t^2} = \frac{\partial^2 \widetilde{E}}{\partial x^2} + k_\omega^2 \widetilde{E} = -\omega^2 \widetilde{P}^{NL} \tag{3.30}$$

The spatial SVEA leads to:

$$\frac{\partial^2 \widetilde{E}}{\partial x^2} \approx exp\left(i\left(k_\omega x - \omega t\right)\right)\left(2ik_\omega\frac{\partial}{\partial x} - k_\omega^2\right)E_\omega + c.c. \tag{3.31}$$

When equations 2.29 and 2.30 are put together and using 2.23 and 2.24 to remove the time dependence as well as the rapid spatial dependency the result is:

$$\frac{\partial E_\omega}{\partial x} = i\frac{\mu_0 c\omega}{2n_\omega}P_\omega^{NL}\,exp\left(-i\Delta kx\right) \tag{3.32}$$

Here the difference in wave vectors between the field and the driving polarization is given by:

$$\Delta k = k_\omega - k_\omega^{'} \tag{3.33}$$

In the more specific case of second harmonic generation, $\Delta k = k_{2\omega} - 2k_\omega$. Applying the d_{eff} convention and noting that $E(-\omega) = E^*(\omega)$, $k(-\omega) = -k(\omega)$, we arrive at the coupled wave equations of second harmonic generation.[61]

$$\frac{\partial E_{2\omega}}{\partial x} = \frac{i\omega}{n_{2\omega}c}d_{eff}E_\omega E_\omega\,exp\left(-i\Delta kx\right) \tag{3.34}$$

$$\frac{\partial E_\omega}{\partial x} = \frac{i\omega}{n_\omega c}d_{eff}E_{2\omega}E_\omega^*\,exp\left(i\Delta kx\right) \tag{3.35}$$

In many practical cases, the conversion efficiencies achieved are very limited. Then the approximation of an undepleted pump light is valid and it is possible to solve the spatial evolution of the second harmonic light analytically by simply integrating equation 2.32 over the crystal length L, resulting in the equation below:

$$I_{2\omega} = \frac{n_{2\omega} c \varepsilon_0}{2} \left| E_{2\omega} \right|^2 = \frac{2\omega^2 d_{eff}^2 L^2 I_\omega^2}{n_\omega^2 n_{2\omega} c^3 \varepsilon_0} sinc^2\left(\frac{\Delta k L}{2} \right) \tag{3.36}$$

The relation between intensity I and electric field E is given in the first part of the equation and the sinc function is defined as sinc(x) = sin(x)/x. Under the plane wave approximation and under the condition of perfect phase matching, we can note that the intensity of the second harmonic wave grows with the square of the fundamental intensity and with the square of the crystal length.

It should be stated here that this derivation was performed for monochromatic light. Most lasers oscillate on a large number of longitudinal modes and the conversion efficiency increases then by a factor of two due to the sum frequency generation between the modes.[67,68,69] The enhancement factor for N modes of equal intensity is 2-1/N. In practice it is rather the case that the theoretically expected conversion efficiency of single longitudinal mode lasers should be decreased by half since the nonlinear coefficients are measured with (cheaper) multi-mode lasers.[70]

An important consequence of equation 2.34 is that the most relevant figure of merit when comparing the conversion efficiency of nonlinear crystals is not d_{eff} but FOM_{NL}, where the subscripts of the refractive indices are removed for simplicity:

$$FOM_{NL} = \frac{d_{eff}^2}{n^3} \tag{3.37}$$

3.6 Phase matching

In order to make a nonlinear process efficient, there are two requirements that need to be fulfilled. The first is energy conservation as shown in equation 2.13 and the other is momentum conservation:

$$\Delta \boldsymbol{k} = \boldsymbol{k}_3 - \boldsymbol{k}_1 - \boldsymbol{k}_2 = 0 \tag{3.38}$$

Here Δk is the momentum mismatch and k_j is the momentum vector for the field at angular frequency ω_j. The phase matching condition can either be fulfilled by the momentum vectors in two (or three) dimensions with non-collinear interacting beams by scalars in the collinear case.[61] In this treatment the case of collinear SHG will be considered.

$$\Delta k = k_{2\omega} - 2k_\omega = 0 \tag{3.39}$$

Due to dispersion in optical materials, the requirement of $n_{2\omega} = n_\omega$ is in general not fulfilled. In the first frequency doubling experiment, the authors were aware of the limited interaction length, but had no means of addressing the issue and the conversion efficiency was thus very low.[12]

When not phase matched, there will be an energy flow from the fundamental wave to the second harmonic wave until they are out of phase by π and then the energy is flowing back

again. The characteristic length over which the second harmonic wave grows is called the coherence length, L_c, of the interaction and is given by:

$$L_c = \left| \frac{\pi}{\Delta k} \right| \tag{3.40}$$

While the energy conservation requirement is fulfilled for all processes at the same time and thus allows all processes simultaneously, phase matching is normally only possible for one process at the time. There are exceptions, though. The trivial ones are those that involve only one wavelength, as in optical rectification or the linear electro-optic effect, or involve a pair-wise degeneracy, as can be the case in four-wave mixing in the third order case. These are automatically phase matched. Another trivial combination is that a process and the reverse process will have the same phase matching conditions. Less trivial is the fact that in quasi phase matched materials there can be several processes of different orders simultaneously phase matched [IV]. More on that in section 4.4.1.

3.7 Birefringent phase matching

There are several ways of achieving phase matching. The most widely used is called birefringent phase matching and was presented independently by Maker *et al.*[71] and Giordmaine[72] very shortly after the first SHG experiment. The technique hinges on the fact that in most crystals the refractive index of the principal crystal axes are different. For normal dispersion $n_{2\omega} > n_{\omega}$, but if the birefringence is large enough it is possible to find a direction where the difference in refractive index for different polarizations can compensate the dispersion.

In uniaxial crystals the refractive index is the same for two of the crystal axes, $n_x = n_y = n_o$, where the o subscript stands for ordinary. Light polarized along the z axis experience the extraordinary refractive index, $n_z = n_e$. For a positive uniaxial crystal $n_e > n_o$ and for a negative uniaxial crystal $n_e < n_o$. The reason for the term uniaxial is that there is only one propagation direction where there is no birefringence, i.e. there is only one optical axis, namely the z axis. When light is propagating at an angle θ to the z axis, then the refractive index of the extraordinary wave is given by:

$$\frac{1}{n_e^2(\theta)} = \frac{\cos^2\theta}{n_o^2} + \frac{\sin^2\theta}{n_e^2} \tag{3.41}$$

Combining this with the relevant Sellmeier equations describing the refractive index there are at most two possible directions phase matched for second harmonic generation in a uniaxial crystal, summarized in table 4.1. For type I phase matching both fundamental photons have the same linear polarisation and for type II phase matching they are of orthogonal polarisations.

	Type I	Type II
Positive uniaxial ($n_e > n_o$)	$n_o(2\omega) = n_e(\omega,\theta)$ (eeo)	$n_o(2\omega) = (n_e(\omega,\theta) + n_o(\omega))/2$ (eoo)
Negative uniaxial ($n_e < n_o$)	$n_e(2\omega,\theta) = n_o(\omega)$ (ooe)	$n_e(2\omega,\theta) = (n_o(\omega) + n_e(\omega,\theta))/2$ (eoe)

Table 3.1. Birefringent phase matching for second harmonic generation in uniaxial crystals.

In figure 3.1 birefringent type I phase matching in a negative uniaxial crystal is illustrated.

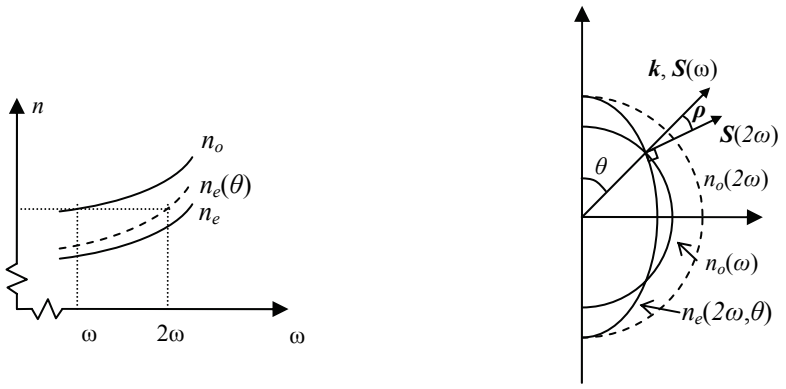

Figure 3.1. Illustration of type I birefringent phase matching in a negative uniaxial crystal. The extra-ordinary refractive index of the second harmonic light with a polarization at an angle of θ to the crystal z axis is equal to the ordinary refractive index of the fundamental wave.

In section 3.5 the general polarization driven vectorial wave equation and a plane wave solution valid under conditions relevant for the thesis work were derived. In the more general case of a plane wave travelling through an anisotropic media, the direction of propagation is given by the wave vector ***k***, and is perpendicular to ***D*** and ***B***. The direction of the energy flow is given by the Poynting vector, ***S***, which is perpendicular to ***E*** and ***H***.[73] If the propagation is not parallel to one of the crystal axes then ***k*** and ***S*** are not parallel and the consequence is that the generated second harmonic will separate from the fundamental beam with distance and the cross section of the second harmonic beam will be elliptical. The walk-off was first dealt with by Kleinman[74] and for type I phase matching in negative uniaxial crystals the walk-off angle ρ is given by:[75]

$$tan\,\rho = \frac{1}{2} n_o^2(\omega)\left(\frac{1}{n_e^2(2\omega)} - \frac{1}{n_o^2(2\omega)}\right) sin(2\theta) \qquad 3.42$$

The walk-off angle means that the beam overlap decreases with distance and there is another critical length that has to be taken into account. This is the aperture length L_a, as given by:[75]

$$L_a = \frac{w_0\sqrt{\pi}}{\rho} \qquad 3.43$$

In the specific case of $\theta = 90°$, called non-critical phase matching, there is no beam walk-off and the angular acceptance bandwidth is larger than for the case of $\theta \neq 90°$, called critical phase matching. Unfortunately, non-critical phase matching is only available for a limited combination of nonlinear materials, temperatures and interacting wavelengths.

Apart from the beam walk-off and the limited angular acceptance, birefringent phase matching has several drawbacks. One is that it cannot be applied on materials with an isotropic refractive index, which for instance excludes the centrosymmetric materials GaAs and ZnSe, two materials of good nonlinearity useful for the infrared region. In general the process involves several dielectric tensor elements. Then an effective nonlinear coefficient d_{eff} must be used, as mentioned in section 2.4. In general the d_{eff} value is lower than all the involved d tensor elements.

In the more general case of a biaxial crystal all three principal axes have different refractive index. Finding phase matching directions and polarisations is more complicated and is treated in detail by Hobden.[76]

Chapter 4

Applied Nonlinear Optics

4.1 Nonlinear crystals

In this section a short overview is given over frequently used materials for frequency conversion in the visible and the near infrared. Potassium titanyl phosphate, $KTiOPO_4$ (KTP), is the material used in the experimental work of this thesis. The properties of bulk and periodically poled KTP (PPKTP) are mainly discussed after the section on quasi phase matching, since the nonlinear optical properties of a periodically poled material hinges on quasi phase matching.

The usefulness of a nonlinear material hinges the fulfilment of several requirements such as high nonlinearity, optical transparency, availability of large single domain crystals of good quality, high damage threshold and the possibility to achieve phase matching.[66] Birefringent phase matching was described in section 3.7 and quasi phase matching will be described in section 4.2.

Although quartz was the material used in the first nonlinear optics experiment it has since then only been used as a reference material for nonlinearity measurements. The nonlinearity is small and the birefringence is too small to permit phase matching. Among the first materials to be used in efficient frequency conversion schemes were the ferroelectric potassium dihydrogen phosphate (KDP) and its isomorph ammonium dihydrogen phosphate (ADP). They were well known from piezoelectric applications, could be grown in large pieces and had high damage thresholds as well as a sufficient birefringence. The nonlinearity was not that high and the crystals were hygroscopic[66]. The transparency range is limited both in the infrared and in the ultraviolet spectral region and other materials appeared, notably the borate crystals. They share many qualities with KDP and ADP including the very high damage threshold but they have a wider transparency range. Two widely used borates are beta-barium borate, β-BaB_2O (BBO) and lithium triborate, LiB_3O_5 (LBO).

Among the ferroelectric materials, lithium niobate, $LiNbO_3$ (LN) and its isomorph lithium tantalate, $LiTaO_3$ (LT) and KTP have been the most frequently used. LN has a large nonlinearity, but the damage threshold is comparatively low due to photo-refraction.

4.2 Quasi phase matching

Quasi phase matching (QPM) is a phase matching technique that achieves phase matching on average. After one coherence length, the generated second harmonic wave and the driving polarization is out of phase by π and the energy starts flowing back to the fundamental wave. In order for the second harmonic wave to keep growing the phase relation must be reset periodically. All the solutions presented in this paragraph were suggested by Armstrong *et al*.[77] in a pioneering article from 1962. One way is to let the interacting waves travel through the nonlinear crystal at an angle in a zigzag fashion and utilize the π phase shift of total internal reflection to reset the phases. In this way the phase resetting is achieved by the optical fields. This can also be done by letting the fields travel through phase correcting linear parts in between the nonlinear regions as is often done in poled glass.[78] It is also possible to reset the phase by changing the sign of the nonlinear coefficient, ideally every coherence length. Since second order nonlinear materials are non-centrosymmetrical this can be achieved by

rotating the nonlinear crystal 180 degrees. This approach was first demonstrated with a stack of rotated quartz wafers by Franken and Ward, who independently suggested the scheme.[79]

Their experimental approach had several drawbacks, the major one being the large reflection losses caused by all the wafer surfaces. Another disadvantage was that for manufacturing reasons the wafers had to be thicker than a coherence length and in their case it was about 20 L_c. Since then the method has been improved with Brewster angled plates[80,81] and diffusion-bonded stacks.[82] A more recent development is QPM in orientation-patterned GaAs grown by a combination of molecular-beam epitaxy and hydride vapor-phase epitaxy.[83]

A somewhat different example of QPM is the use of the third-order DC-induced second harmonic effect in a liquid nitrobenzene waveguide with periodic electrodes.[84]

In ferroelectrics, periodic structures for QPM have been fabricated in several different ways. In LN, periodic domain reversal was achieved during crystal growth.[85] Ion-exchange in waveguides[86] and electron beam writing[87] are two other methods that have been used.

The big step forward in QPM technology and usage came with the electric field poling of ferroelectrics. Yamada *et al*.[88] were the first to achieve electric field periodic poling in waveguide LN in 1992 and very soon bulk poling was achieved.[89] In KTP the electric field periodic poling started with the results by Chen and Risk[90] and by Karlsson and Laurell.[91] The poling process of KTP with isomorphs has since then been extensively studied and presented in several doctoral theses at KTH.[92,93,94,95] Since the early days, electric field periodic poling has developed into a reasonably mature technology with commercial production of nonlinear crystals. The list of crystals available for QPM has grown steadily over the years. This is not only because of the search for new materials including isomorphs of known crystals, but also because of improvements in the crystal fabrication and the introduction of dopants in known materials.

4.2.1 The theory of quasi phase matching

With a nonlinear coefficient varying with position, $d = d(x)$, equation 3.34 is no longer valid but has to be modified. In the general case the solution is to include the nonlinear coefficient in the spatial integration. If the modulation of d is periodic, Fourier techniques can be used in order to simplify the calculations. Assuming $-1 < g(x) < 1$, the following treatment covers all types of QPM with periodicity Λ.

$$d(x) = d\,g(x) = d\sum_{m=-\infty}^{\infty} G_m \exp\left(-\frac{2\pi i m x}{\Lambda}\right) \qquad 4.1$$

In this expression the subscript m is the order of the QPM, G_m is the Fourier coefficient of order m, and Λ is the period of the pattern. In principle the nonlinear coefficient d used can in itself be an effective nonlinearity d_{eff}, as in GaAs,[80,81] but in the most widely used cases the single d coefficient with highest nonlinearity (e.g. d_{33} in PPLN and PPKTP) is used. In the following I will use the notation of a grating momentum vector K_m, as defined below. This simplifies the expression for momentum conservation.

$$K_m = \frac{2\pi m}{\Lambda} \qquad 4.2$$

The growth of the second harmonic field is then given by:

$$E_{2\omega} = \frac{i\omega E_{\omega}^2}{n_{2\omega}c} d \int_0^L \sum_{m=-\infty}^{\infty} G_m \exp\left(i\left(\Delta k - K_m\right)x\right)dx \qquad 4.3$$

The only substantial contribution to the integral comes from the grating vector or vectors that fulfil:

$$\Delta k_Q = \Delta k - K_m \approx 0 \qquad 4.4$$

It should be noted that in equation 4.3, the d coefficient is outside the integral. Thus the grating structure variations will influence all processes of the same order in the same way. The most common QPM structures are those where the $g(x)$ switches periodically between -1 and 1. Consider the case of a rectangular structure with a duty cycle of $D = l / \Lambda$. This means that $g = 1$ for a distance of l and $g = -1$ for the rest of the period. The Fourier coefficients are then given by:

$$G_m = \frac{2}{\pi m} \sin\left(\pi m D\right) \qquad 4.5$$

From this it is clear that the most efficient phase matching comes from $m = \pm 1$ and $D = 0.5$. Then equation 3.36 is valid under the modified d_{eff} expression and the substitution $\Delta k \rightarrow \Delta k_Q$.

$$d_{eff} = \frac{2d}{m\pi} \sin\left(\pi m D\right) \qquad 4.6$$

$$I_{2\omega} = \frac{2\omega^2 d_{eff}^2 L^2 I_{\omega}^2}{n_{\omega}^2 n_{2\omega} c^3 \varepsilon_0} sinc^2\left(\frac{\Delta k_Q L}{2}\right) \qquad 4.7$$

It should be stated that the squared sinc dependency is only valid for plane waves. The consequences of strong focussing in terms of optimum phase matching are discussed in section 4.6. Another observation is that the squared sinc shape is a consequence of the grating design and it is thus possible to design the structure for other phase matching shapes.[96] The full width half max acceptance bandwidth of equation 3.10 is given by:

$$\frac{\Delta k_Q L}{2} = 0.4429\pi \qquad 4.8$$

The source of the phase mismatch can be a detuning of one or several of the following parameters: grating period, temperature, wavelength or angle. The theoretical analysis for the full width half max bandwidth $\delta\zeta$ in terms of the relevant parameter ζ can be found in the article by Fejer *et al*.[97]

$$\delta\zeta = \frac{5.57}{L} \left| \frac{\partial \Delta k}{\partial \zeta} \right|^{-1} \qquad 4.9$$

This article also deals with imperfect structures, for instance grating with missing domains or random variations of the domain wall positions.

4.3 Periodically poled potassium titanyl phosphate

KTP is the nonlinear material that has been used throughout the work of this thesis. The bulk crystal is orthorhombic of the point group[98] mm2, which means that it is non-centrosymmetric and thus the material exhibits a non-zero second order nonlinearity. The crystal symmetry allows for five nonzero d-coefficients, the values of which are given in table 4.1.[99] Another direct consequence of the crystal structure is that the material is anisotropic – it is biaxial with different refractive indices along the three crystallographic axes. Several authors[100,101,102] have reported on refractive index data for KTP and in this thesis mainly the values of Fan *et al.*[100] have been used for dispersion calculations. The Sellmeier equation for z polarized light is given in table 4.2. For temperature tuning calculations the dependencies supplied by Wiechmann *et al.*[103] were used as well as thermal expansion coefficients[104], see table 4.3.

Crystal	d_{15} [pm/V]	d_{24} [pm/V]	d_{31} [pm/V]	d_{32} [pm/V]	d_{33} [pm/V]
KTP	1.9	3.6	2.5	4.4	16.9

Table 4.1 Nonlinear optic coefficients of KTP, measured at λ = 1064 nm.[99]

Sellmeier equation, λ in μm: $n^2 = A + \frac{B}{1 - C/\lambda^2} - D\lambda^2$

Crystal	A [-]	B [-]	C [μm^2]	D [μm^{-2}]
KTP, z axis	2.25411	1.06543	0.05486	0.02140

Table 4.2 Sellmeier equation coefficients of KTP, suited for λ < 1 μm.[100]

Temperature dependence of refractive index, λ in μm: $\frac{dn}{dT} = \frac{a}{\lambda^3} + \frac{b}{\lambda^2} + \frac{c}{\lambda} + d$

Crystal	a [$\mu m^3 K^{-1}$]	b [$\mu m^2 K^{-1}$]	c [$\mu m K^{-1}$]	d [K^{-1}]	Thermal exp.[K^{-1}], x-axis
KTP, z-axis	$12.415*10^{-6}$	$-44.414*10^{-6}$	$59.129*10^{-6}$	$-12.101*10^{-6}$	$11*10^{-6}$

Table 4.3 Temperature dependencies for KTP.[103,104]

From a more practical point of view, the following properties should be stressed. KTP has excellent optical and mechanical properties. The damage threshold is large and the crystal has no water absorption. KTP has a large transparency window, ranging from 365 nm to approximately 4.3 μm.[105] The material has also the benefit of a large temperature and wavelength bandwidth.

KTP is ferroelectric and can thus be poled. The electric field necessary to invert the domains is smaller by an order of magnitude than that needed for inverting domains in LN. The spontaneous polarisation is directed along the crystal z axis and the poling reverses the polarisation. Domain walls preferentially formed parallel to the y-z-plane, since this is energetically favourable.[106] The corresponding grating vector in a PPKTP crystal is thus aligned in the crystal x direction, which facilitates the use of the nonlinear coefficients d_{33}, d_{24} and d_{32}. In practice, only the largest nonlinear coefficient d_{33} is employed and even though the

effective nonlinearity d_{eff} is smaller by a factor of $2/\pi$ for first order interactions, it is still much larger than the d_{eff} of birefringent phase matched interactions. The periodically poled flux grown KTP crystals used in this work were all fabricated by the electric field poling process developed by Karlsson and Laurell.[91] Periodic poling with grating periods in the range of 3.4 – 36 μm covers most first order QPM processes within the transparency window.

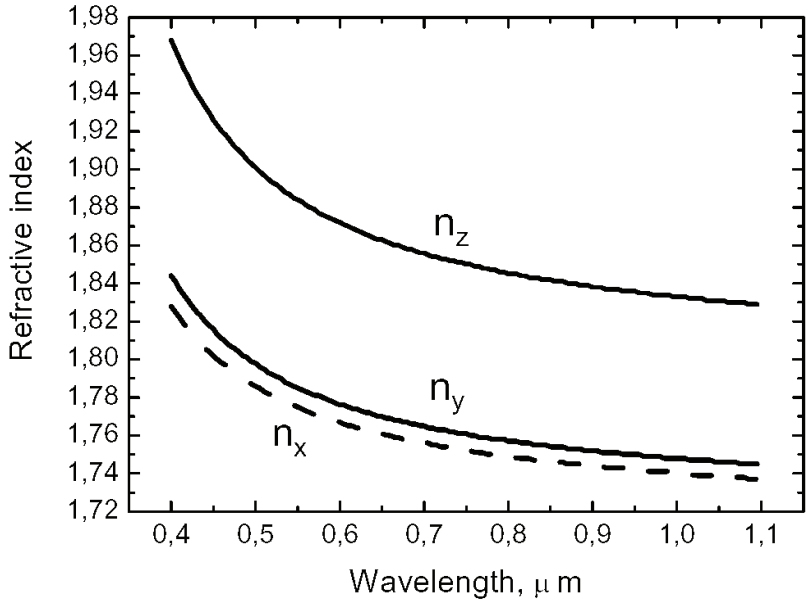

Figure 4.1. Dispersion of the refractive index in KTP.

Flux grown KTP crystals varies in stoichiometry and the most notable consequence is the substantially variation of crystal conductivity, a property that has a significant influence on electric field poling. The poling procedure is a nontrivial task with many parameters and in many instances nonuniform ferroelectric domain nucleation and domain broadening occur, which decrease the quality of the poled structure and hence the effective nonlinearity of the poled crystals.

The most common method of characterizing PPKTP is to test the performance of the crystal directly in the appropriate sum- or difference-frequency generation configuration, finding out effective nonlinearities and effective crystal lengths.[95] For OPO crystals in particular, it can be more convenient to test the crystal by utilizing second harmonic generation in high order QPM.[107]

Another common method of assessing the quality of a periodically poled crystal is to use a selective chemical etching. The etching rate is different on the two polar faces of the crystal which reveals the domains. The technique was demonstrated in LN by Nassau *et al*. in 1965[108] and in KTP by Laurell *et al*. in 1992.[109] In the article from 1992 other characterization methods based on piezoelectricity, surface SHG and pyro-electricity are also shown. Methods of considerably higher spatial resolution include the use of atomic force microscopy in different configurations.[94] These are time consuming techniques but very useful for fundamental research on domain inversion. There are also live imaging techniques available.[110,111,112]

4.4 Second harmonic generation in QPM PPKTP

The general phase matching condition of a second harmonic process is given by:

$$\Delta k_Q = \Delta k - K_m = \frac{4\pi n_i(2\omega)}{\lambda} - \frac{2\pi n_k(\omega)}{\lambda} - \frac{2\pi n_l(\omega)}{\lambda} - \frac{2\pi m_{ij}}{\Lambda} \approx 0 \qquad 4.10$$

Here λ is the vacuum wavelength of the fundamental beam, i, j, k and l are Cartesian coordinates as defined in equation 3.15 and m_{ij} is the order of the QPM corresponding to the d-coefficient d_{ij}. For a given period Λ there can be several different processes phase matched. For instance, long period gratings for infrared OPO's utilising the type I d_{33} nonlinear coefficient can be tested by high-order ($m_{ij} > 1$) SHG into the visible using d_{33}. This is frequently done during poling. Moreover, every grating period used can be used for first-order SHG utilising the type II d_{24} with fundamental wavelengths covered by a commercial standard Ti:Sapphire laser. A simple, but typical, set-up for second harmonic generation is depicted in figure 4.2 below. The laser emits linearly polarized light and if needed a half wave plate is used for polarization rotation. A linear polarizer adds to the functionality by allowing power adjustment without changing the output of the laser. Lenses are used for focussing the fundamental light into the nonlinear crystal and if needed for collimating the light after the crystal. A filter is used to separate the second harmonic light from the fundamental beam. For temperature tuning purposes, the crystal holder temperature is controlled by a peltier element.

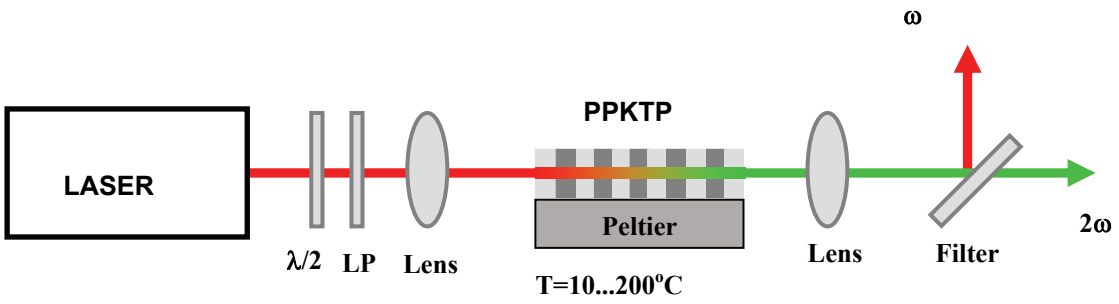

Figure 4.2. Standard setup for SHG. LP – linear polarizer. λ/2 – half wave plate.

4.4.1 Simultaneous phase matching of several second order processes

PPKTP is normally poled with the grating vector parallel to the x crystallographic axis. Looking at table 3.2 and equation 2.16 we find that the nonlinear coefficients d_{33}, d_{24} and d_{32} are available for collinear QPM. The d_{33} coefficient is the most widely used, since the nonlinearity is highest. Second harmonic generation employing d_{33} is a type I process, producing z-polarized second harmonic light from an incident z-polarized fundamental beam. The type I d_{32} process is the least efficient but is of some interest nonetheless, since it produces a second harmonic beam that is orthogonal to the fundamental beam. When doubling into the blue spectral region the first order QPM period of the type II d_{24} process is significantly larger than those of the type-I coefficients, thereby making it easier to produce homogeneously poled crystals. The type II d_{24} process also has the benefit of a larger phase-matching bandwidth.[113]

Looking at equation 4.10, it can be used to calculate the QPM period Λ for different orders of all the three different SHG processes in PPKTP. This was done in the wavelength region of 0.7 - 1.1 μm, a span covered by Ti:Sapphire lasers, and the resulting phase matching curves are shown in figure 4.3.

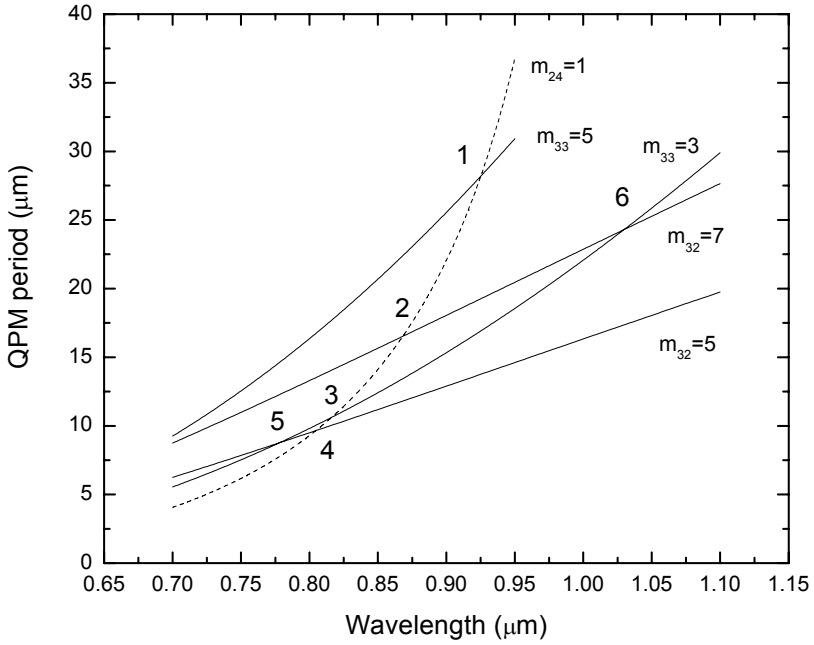

Figure 4.3. Phase matching curves for SHG in PPKTP accessible by Ti:Sapphire pumping.

The most striking feature of this graph is the crossing points 1-6, where it is possible to generate simultaneous QPM SHG with two different nonlinear coefficients. In particular, it is possible to achieve collinear simultaneous type I and type II SHG, something that is not possible in birefringent phase matching. In the article [IV], the crossing points labelled 1 and 3 are investigated in more detail. These are crossings where the quotient between the effective nonlinearities of the two involved processes is close to one. It is shown that it possible to rotate the polarization of the second harmonic beam by tuning the polarization of the fundamental field, see figure 4.4 (a). Moreover, if the fundamental polarisation allows for both processes, it is possible to change the ratio between the second harmonic polarizations by temperature tuning the PPKTP crystal, as shown in fig. 4.4 (b). For these experiments we used a set-up looking like that depicted in fig. 4.2 and a mode-locked Ti:Sapphire laser.

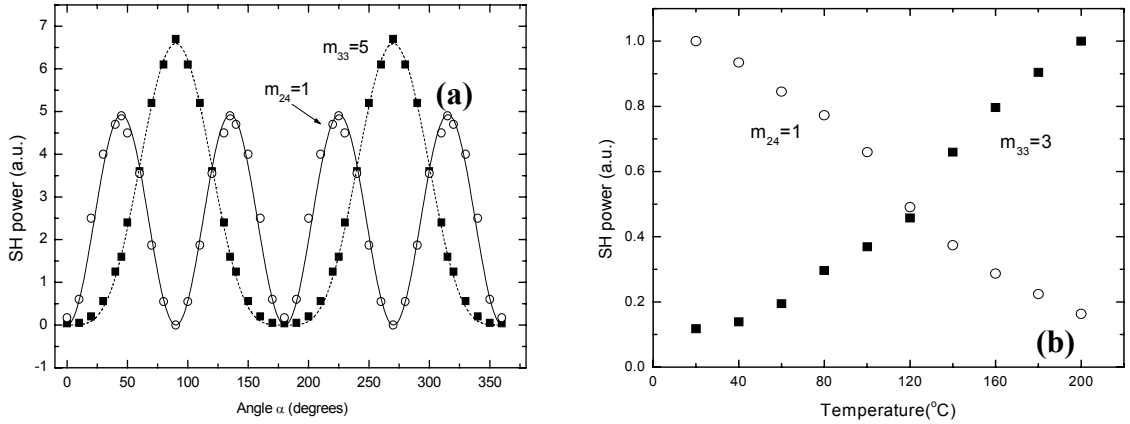

Figure 4.4. Change in the second harmonic power by (a) rotating the fundamental polarization or by (b) changing the temperature of the nonlinear crystal.

In the type II case the conversion efficiency of femtosecond pulses is limited by the group velocity mismatch between the two fundamental beams, i.e. the fact that the different group velocities causes a physical separation between the pulses of orthogonal polarizations and the SHG ceases. This phenomenon can be utilized to gain knowledge on the properties of periodically poled materials and type II bulk materials as is shown in the next passage.

4.4.2 Three dimensional characterization of nonlinear crystals

The two most commonly used methods of characterizing periodically poled crystals mentioned in the end of section 4.3, selective etching and direct optical characterization by first order or high order SHG, both have their drawbacks. Selective etching is a surface method, giving data on the domains on the surface only. The poling quality and the duty cycle inside the crystal can be substantially different.[114] As for the direct measurement of second harmonic power the main drawback is that it only provides information on the effective nonlinearity integrated along the full optical beam path. If a higher order quasi phase matching is used for the characterization the results should be interpreted remembering the difference of sensitivity of the duty cycle, as seen by equation 4.6. Since the poled structure can be non-uniform along the beam path, with missing domains as well as difference in duty cycle, a method for investigation the quality of the poled structure in three dimensions is desirable. This can be realised by SHG in the overlap volume of two tightly focussed beams[115] or by taking advantage of the group velocity mismatch between the two orthogonally polarized short fundamental pulses in a type II SHG configuration [V].

The principle is quite simple. In type II SHG, two orthogonally polarized fundamental waves interact. When short pulses are used, the difference in group velocity will cause the pulses to separate and the interaction length is limited to region where the pulses overlap. Thus the generated second harmonic reflects a local nonlinearity and the spatial resolution along the beam propagation is given by the group velocity mismatch limited interaction length, L'_{GVM}:

$$L'_{GVM} = \frac{ct_p}{\left|n_{g,z}(\omega) - n_{g,y}(\omega)\right|} \qquad 4.11$$

If the pulse of the polarization with largest group velocity is delayed with respect to the orthogonally polarized pulse by a distance x_d, then delayed pulse will have caught up after a distance of x_c and the relation between x_c and x_d is given by:

$$x_c = \frac{x_d}{n_{g,z}(\omega) - n_{g,y}(\omega)} \qquad 4.12$$

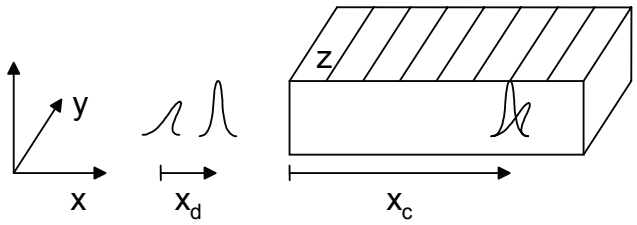

Figure 4.5. By adjusting the delay distance x_d the position of interaction x_c can be chosen.

Spatial resolution in the transverse direction is achieved by imaging the second harmonic light and the actual value will depend on imaging conditions such as magnification, pixel size,

numerical aperture of imaging lens etc. So by a taking a set of pictures at different delays a three dimensional map of the nonlinearity can be created.

Looking at the dotted line in figure 4.3, showing the phase matching curve for first-order type II SHG in PPKTP using the d_{24} nonlinear coefficient it is clear that with a Ti-Sapphire laser one can cover all grating sizes between 5 μm and 40 μm i.e. almost every period used in practical QPM structures.

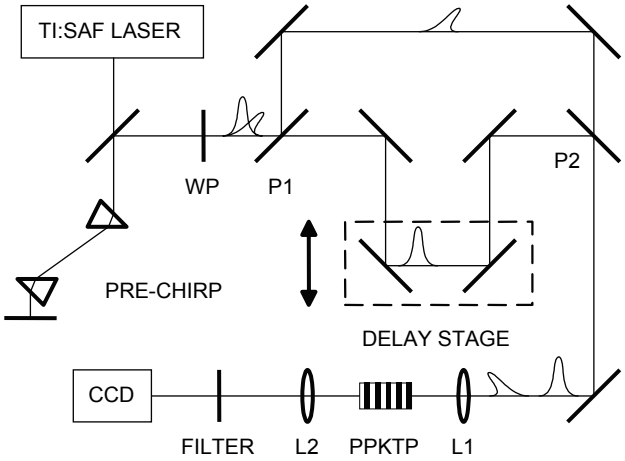

Figure 4.6, Experimental setup. The routing of the fs pulses is explained in the text.

The experimental realization of the 3D characterization scheme was done with the setup depicted in figure 4.6. A Ti:Sapphire laser generating 80 fs pulses at an 80 MHz repetition rate was the source of the fundamental pulses. The pulses were then prechirped by a double pass through a two prism arrangement,[50] in order to compensate for the temporal pulse broadening by the normal dispersion of various optics prior to the nonlinear crystal. A half-wave plate was used to rotate the polarization to 45° relative to the PPKTP z axis and the two polarizations were separated by a polarizing beam splitter. The y-polarized light was then routed by an adjustable delay stage and the two polarizations were then brought together by another polarizing beam splitter. A lens brought the beam to a weak focus inside the crystal and a second lens was used to image the second harmonic light upon the CCD matrix. Suitable filters were used to block the fundamental beam and by changing the delay a set of two dimensional frames formed a three dimensional map of the effective nonlinearity. A 4 mm long PPKTP crystal of period 9.01 μm was investigated with a longitudinal resolution of 285 μm and transversal resolution of ~ 7.5 μm, limited by the aperture of the imaging lens. Since the pulse length broadens in the crystal due to group velocity dispersion, the longitudinal resolution will increase with distance. This was not a problem in the experiment, since the dispersion length was more than twice the length of the crystal. The effect of dispersion and possible remedies are discussed in the article [V] The background of non-phase matched type I SHG was subtracted from the images and by calculating the square root of the second harmonic intensity, values proportional to the effective nonlinearity were achieved. Four frames separated by 0.75 mm are shown in figure 4.7. The grey scale is proportional to the local value of d_{eff}.

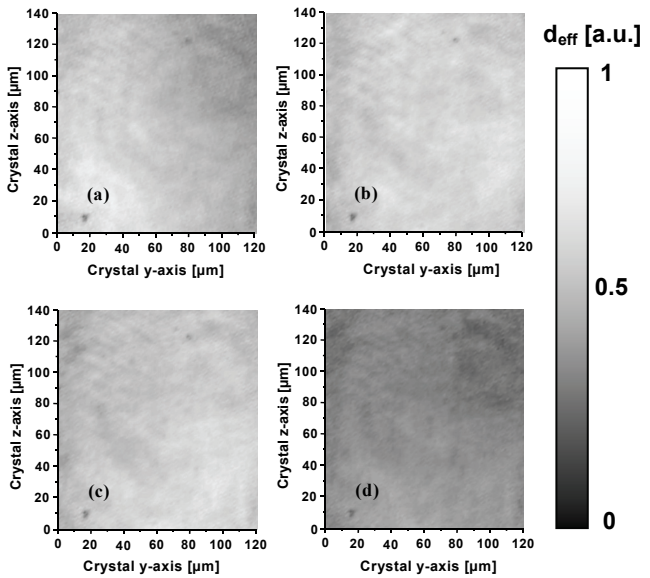

Figure 4.7. Measured distribution of the effective nonlinearity in PPKTP. The distance between subsequent frames is 0.75 mm along the crystal x axis.

Both the effective d_{33} and the effective d_{24} nonlinearity depend only on the quality of the grating structure and the quality of the bulk crystal. Assuming the bulk crystal contribution to be negligible, and in the case of using the same order m for both interactions, it is possible to achieve absolute values of both the effective d_{33} and the effective d_{24} nonlinearity by calibrating the measured $d_{24eff}(x)$ dependency to an independent CW type I SHG experiment. Figure 4.8 shows $d_{33eff}(x)$ for the whole crystal length obtained in this way.

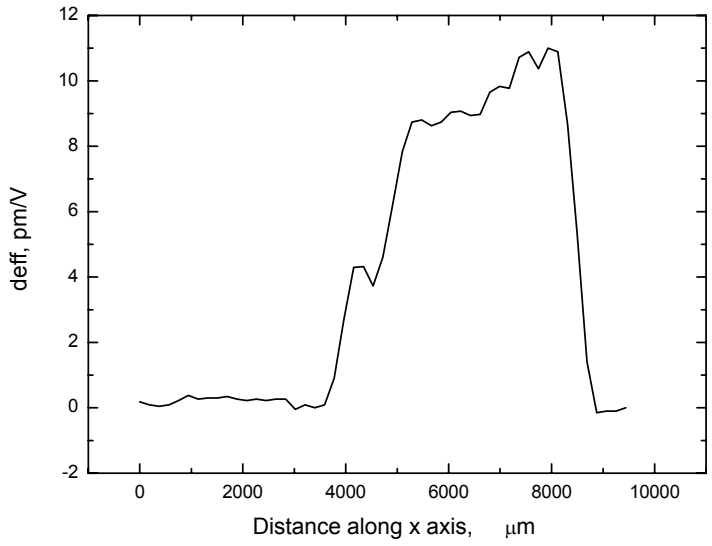

Figure 4.8. Distribution of the effective nonlinearity $d33_{eff}$ along the PPKTP x axis.

The method demonstrated can be used for any PP material as well as for 3D characterization of bulk type II crystals. In periodically poled crystals the high longitudinal resolution is particularly important when characterizing crystals with several different grating periods, such as tandem gratings for THG or chirped gratings.

4.5 Pump depletion

The treatment in chapter three is not valid when the pump light is depleted. Armstrong *et al*.[77] demonstrated in 1962 that with a suitable variable substitution the coupled wave equations (3.34-35) will have a single coupling factor and can then be solved analytically.[14] The result under perfect phase matching and for a plane wave is that the intensity of the second harmonic wave grows with a $\tanh^2$ dependency of distance:

$$\eta = \frac{I_{2\omega}}{I_{\omega}} = tanh^2\left(\frac{L}{L_{NL}}\right) \qquad 4.13$$

L_{NL} is the nonlinear length scale and is a measure of the nonlinearity of the interaction. The conversion efficiency is 58% when the crystal is L_{NL} long. For a plane wave L_{NL} is inversely proportional to the fundamental intensity I_{ω} and inversely proportional to the square root of the nonlinear figure of merit FOM_{NL}.[61] The effect of pump depletion needs to be taken into account in high power CW applications as well as when the fundamental wave is pulsed.

4.6 Focussed Gaussian beams

In general, laser beams have a Gaussian spatial intensity distribution.[15] Thus the plane wave treatment of chapter 3 is not fully valid. In particular, knowing that the intensity of a beam is given by the power divided by the area, $I = P / A$, equation 3.36 gives the impression of higher second harmonic powers for tighter focussing. This is not true, since diffraction of the beam limits the effective interaction length. Kleinman *et al*.[116] defines an effective length of focus, L_f, related to the confocal parameter b by:

$$L_f = \frac{\pi b}{2} \qquad 4.14$$

Optimum focussing is thus a trade-off between high intensity and long interaction length. Assuming focussing conditions so that L_f is always equal to the crystal length L and knowing that b is proportional to the area at the foci; one should expect $I_{2\omega}$ to be linearly dependent on L. This is in contrast to the quadratic dependence exhibited by plane waves and beams confined in waveguides and fibres. Another expected difference is that since b is proportional to the refractive index, then the relevant figure of merit should be d_{eff} squared divided by the refractive index n squared. A full theoretical analysis performed by Boyd and Kleinman[117] confirms the expectations:

$$\eta = \frac{16\pi^2 P_{\omega} d_{eff}^2}{\varepsilon_0 c \lambda_{\omega}^3 n_{\omega} n_{2\omega}} L\, h_m(B,\xi) \qquad 4.15$$

Here h_m is the Boyd Kleinman focussing factor in the case of no pump depletion, no absorption, with optimized phase mismatch and the foci in the centre of the nonlinear crystal. The optimum focussing condition when there is no angular walk-off ($B = 0$) is $\xi = L/b = 2.84$, with $h_m = 1.054$.

In the case of strong focussing the squared sinc shape becomes distorted and the optimum value of Δk or Δk_Q changes from zero to a negative value in the sign convention used in this thesis.[117] The reason for this is that phase matching is a vector condition and in a strongly

focussed beam the vector sum of two longer wave vectors can be equal to the sum of two shorter collinear wave vectors, as seen in figure 4.9.

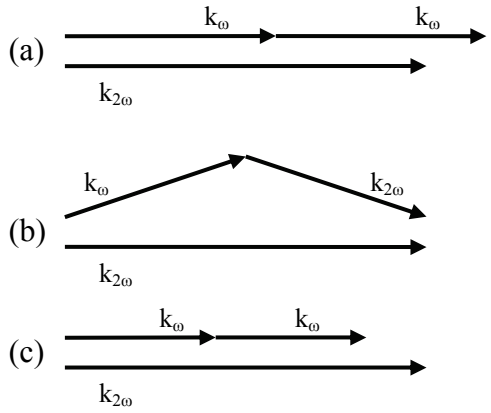

Figure 4.9. (a) Phase matching with negative Δk. In a strongly focussed interaction, the fundamental beam will contain an angular spread of wave vectors and thus the case of (b) can be efficient. (c) For a positive Δk, the interaction will never be efficient.

The focussing conditions for CW type II SHG has also been studied[118,119] with the main result being that the results coincide with those for type I SHG when there is no birefringence, but with increased birefringence the type II efficiency drops more quickly, but on the other hand the focussing is less important. The problem of decreased efficiency with birefringence can be addressed by using an elliptic focussed beam.[120,121]

4.7 Short pulses and thick crystals

The Boyd-Kleinman results in section 4.6 are valid for continuous wave interaction and in practice for quasi-CW and for long pulses. For short pulses though, the difference in group velocity between the fundamental pulse and the generated second harmonic pulse will cause a degradation of the performance. When the crystal is long compared to the group-velocity mismatch length L_{GVM}, also known as the nonstationary length L_{nst}, then the results in section 4.6 are not valid any longer.

$$L_{GVM} = L_{nst} = \frac{t_p}{v_g^{-1}(2\omega) - v_g^{-1}(\omega)} = \frac{ct_p}{n_g(2\omega) - n_g(\omega)} \qquad 4.16$$

In particular, for loose focussing, $\xi < 1$, the characteristics of the second harmonic generation differs depending on whether the crystal is long or short. For short crystals, $L << L_{GVM}$, the second harmonic will be shorter than the fundamental pulse and the power will depend quadratically on the crystal length. For long crystals, $L << L_{GVM}$, the dependency is linear and the second harmonic pulse length scales linearly too.[30]

The analysis of Boyd and Kleinman was extended to the thick crystal regime by Saltiel *et al.*[122] The results show that with increased group velocity mismatch the conversion efficiency drops and a tighter focussing is needed for optimum conversion. The drop in conversion efficiency is compensated by the peak intensities available in femtosecond pulses and the overall conversion efficiency can be high.

4.7.1 Efficient SHG of fs pulses in PPKTP

The laser source used in this SHG experiment [III] was a diode-pumped femtosecond Yb:KYW laser,[123] passively mode locked by a semiconductor saturable absorber mirror. The laser produced fundamental pulses of 130-140 fs duration in the 1040-1050 nm wavelength range at a repetition rate of 78 MHz with an average output power of 240-320 mW. The fundamental wave was frequency doubled in a set-up like the one in figure 4.2. The nonlinear crystals used were a 4.8 mm long PPKTP with a period of 8.34 μm and a 2.7 mm long aperiodically poled KTP (APPKTP) crystal with a linearly chirped grating with periods ranging from 8.24 μm to 8.44 μm. The crystals were used in type I SHG utilising the d_{33} nonlinear coefficient. For this process and the fundamental pulse lengths used, the group velocity mismatch length L_{GVM} is about 200 μm, so the crystals are hence thick. In spite of this, a conversion efficiency of up to 64% was achieved, see figure 4.10 (a).

A thorough investigation was performed on of the influence of crystal temperature on second harmonic efficiency as well as the influence of focussing on such second harmonic properties as pulse lengths, spectral bandwidth and average powers. Some of the results will be discussed in the paragraph below.

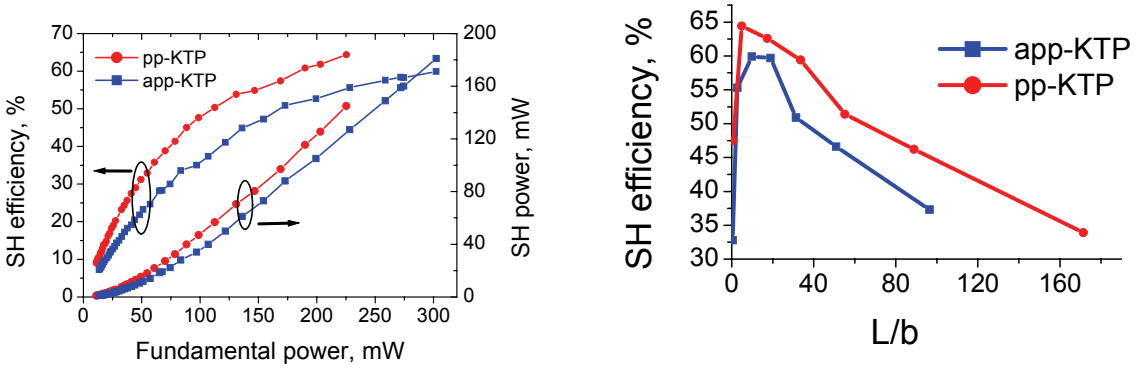

(a) (b)

Figure 4.10. (a) Conversion efficiency and second harmonic power. (b) Conversion efficiency as function of L / b ratio.

The optimum focussing condition depends on which property of the second harmonic light is most important for the application at hand. For very short second harmonic pulses, the interaction length must be short and thus a very high L/b ratio must be used. In the experiment we achieved second harmonic pulse lengths as short as 177 fs, i.e. 1.4 times the fundamental pulse length, with a L/b ratio of 96 in the APPKTP crystal. For this we used the strongest lens we had available. On the other hand, if the second harmonic output power is the most important parameter then the optimum focussing is looser, with L/b ~ 5-10. 180 mW of average green power with a conversion efficiency of 60% was achieved using the PPKTP crystal and with the APPKTP crystal a maximum of 145 mW was generated with a conversion efficiency of 64%. These results are shown in figure 4.10 (a) and there was clear evidence of pump depletion at high fundamental powers under all focussing conditions. For the case when the main priority is high peak power in the second harmonic, e.g. for further frequency conversion, then an intermediate focussing is the optimum with L/b ~ 50. The dependency of the L/b ratio in three cases are seen in figures 4.10 (b), 4.11 (a) and 4.11 (b).

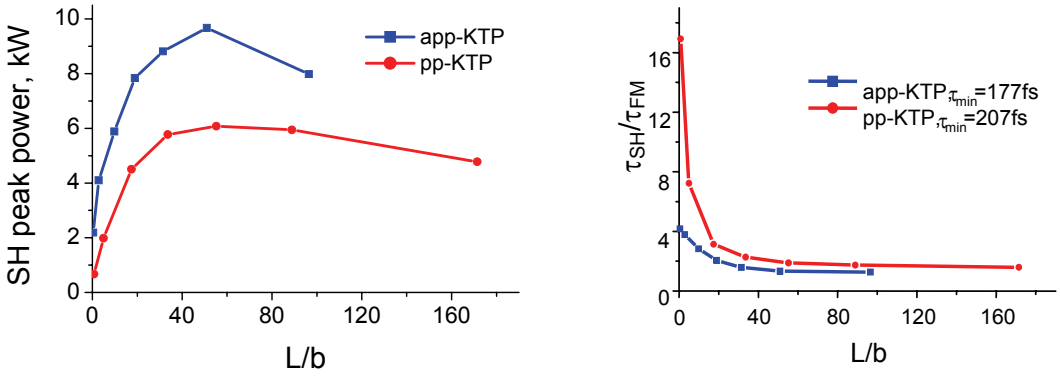

(a) (b)

Figure 4.11 (a) Peak power dependency of L / b ratio. (b) Pulse width dependency on L / b ratio.

4.8 Cascaded second order interactions

Third order effects can often be effectively mimicked by the cascading of two second order effects. The simplest example is third harmonic generation in two steps – second harmonic generation followed by sum frequency generation between the second harmonic wave and the fundamental wave. Since the second order nonlinearity is stronger than the third order, it can be beneficial to use cascaded processes. In this passage it will be shown that the cascading of second harmonic generation and difference frequency generation creates a nonlinear phase contribution or, in other words, an effective nonlinear index of refraction.

In chapter three, the coupled wave equations (equations 3.34 and 3.35) for second harmonic generation were derived. Under the assumption of no pump depletion and no initial second harmonic the second harmonic wave at a position x is given by the integration of 3.34:

$$E_{2\omega}(x) = i\frac{\omega}{n_{2\omega}c} d_{eff}\, x\, exp\left(\frac{-i\Delta kx}{2}\right) sinc\left(\frac{\Delta kx}{2}\right) E_{\omega}^{2} \qquad 4.17$$

Substituting this back into 3.35 renders the following expression for the fundamental:

$$\frac{\partial E_{\omega}}{\partial x} = -\frac{\omega^2 d_{eff}^2}{n_{\omega} n_{2\omega} c^2}\, x\, exp\left(\frac{i\Delta kx}{2}\right) sinc\left(\frac{\Delta kx}{2}\right) \left|E_{\omega}\right|^2 E_{\omega} \qquad 4.18$$

The exponential term implies a real and an imaginary part – i.e. there is both a phase shift and a loss term. The loss is simply the remaining second harmonic light. The phase shift is not due to a real change in the refractive index but is a consequence of that the light has travelled some distance at a different phase velocity as a second harmonic wave. Thus if a second beam of light would pass through the same sample at the same time it would not be affected. The beam producing the phase shift will see an effective nonlinear index of refraction, n_2. In a crystal of length L this is given by:[124]

$$n_2^{eff} = \frac{2\omega d_{eff}^2}{n_\omega^2 n_{2\omega} c^2 \varepsilon_0} \frac{(sinc(\Delta kL) - 1)}{\Delta kL} L \qquad 4.19$$

Note that the effective n_2 is proportional to the FOM_{NL} of second order materials, thus the nonlinearity of the effective third order process emulated by cascaded second order processes can be much more efficient than the true third order equivalent. By changing the phase mismatch Δk, both the amplitude and the sign of the effective n_2 can be altered. The price of this flexibility is that the process is not automatically phase matched, which is the case of the third order n_2. The approximation of no pump depletion will break down at higher intensities and then the difference between true third order n_2 and the effective n_2 from cascading will be apparent. Numerical simulations show that the phase shift will be distorted due to saturation and that this can be compensated for by using a larger phase mismatch and a higher intensity.[125] A second short-coming of the description above is that the effect of group velocity mismatch is not taken into consideration, an effect that causes further distortions.[126] The remedy is to keep the phase mismatch so large that the cycle of conversion and back conversion takes place in less than a group velocity mismatch length.[125] A difference between the model and a real cascaded Kerr lens situation is that the wave front is not normally flat but curved.

4.8.1 Cascaded Kerr lens mode locking

In article [I] we demonstrated a cascaded Kerr lens mode locked Nd:$GdVO_4$ laser. The laser (see figure 4.12 (a)) is a four mirror z-folded cavity with two intra cavity foci at the flat end mirrors. The intracavity distances and further details on the cavity elements can be found in the article. The nonlinear lensing employed in this cavity is defocusing, in contrast to the ordinary Kerr effect.

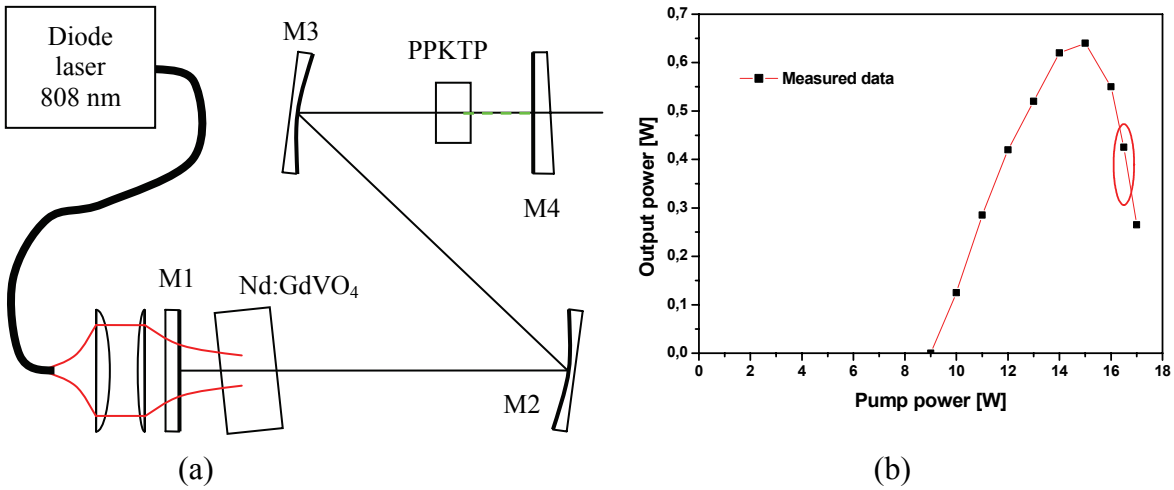

(a) (b)

Figure 4.12 (a) Cavity design. M1 though M4 – cavity mirrors. (b) Output power versus fibre-coupled diode power. The ellipse marks the region of mode locked operation.

In order to mode lock, the cavity must be operated close to its stability limit. This is a general rule of Kerr lens mode locking.[127] This was achieved by decreasing the pump spot size from the size of maximum CW output power to a smaller size. Thereby the thermal lens power in the active media was increased by a factor of approximately 1.8 and the laser worked in the thermal roll-off regime indicating large intracavity losses (see fig. 4.12 (b)). The cavity is believed to work in the geometrically unstable regime, though the thermal lens measurements

were not conclusive. Simulations show that regardless of geometrical stability, a negative cascaded Kerr lens (CKL) counteracts the detrimental effects of the strong thermal lens. The implications are an improved mode overlap, an increased geometrical stability of the cavity and reduced round trip losses. If the cavity is geometrically stable, then the diffraction losses are decreased by an increased CKL negative power. On the other hand, if it is geometrically unstable, then the CKL reduces or even cancels the round trip magnification and consequently greatly reduces the diffraction losses. The improved mode overlap and the decrease in round trip losses caused by the CKL provide the mechanism for mode locking.

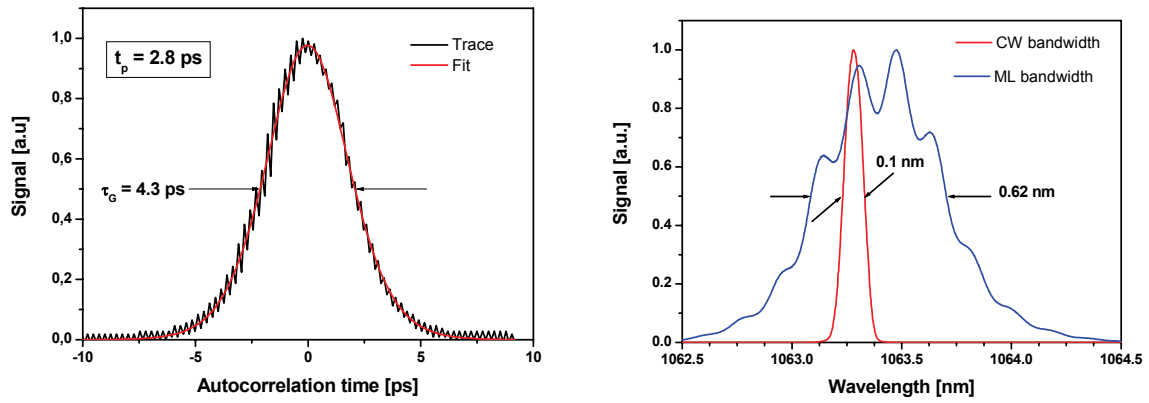

(a) (b)

Figure 4.13. (a) Autocorrelation trace. (b) Spectral bandwidth of CW and mode locked laser.

The laser produced mode locked 1.5 times transform-limited pulses as short as 2.8 ps, assuming a sech^2 pulse shape. An autocorrelation trace is shown in figure 4.13 (a) and in figure 4.13 (b) the spectral width is shown for both CW and mode locked operation. When the laser was mode locked the bandwidth increased by more than 6 times to a FWHM bandwidth of 0.62 nm, indicating that the entire spectral gain bandwidth was mode locked. The modulation of the spectrum comes from the cascaded phase shift. The repetition rate of the laser was 200 MHz and the average power 350 mW.

A full description of the cascaded Kerr lensing includes the effects of a curved wave front as well as the group velocity mismatch between the fundamental and the second harmonic pulses. The influence of these factors was studied by numerical simulations using the software package SNLO.[128] One important finding is that for a focussed beam the GVM enhances the strength of the cascaded Kerr lens compared to the case of no GVM. Furthermore, the Kerr lensing becomes bipolar over the pulse length, i.e. the leading edge and the trailing edge experience cascaded Kerr lensing of different signs. This provides a very strong pulse shortening effect – the leading edge experience focussing and increased diffraction losses and the trailing edge experience defocusing with decreased diffraction losses. The reason for the temporal shift for the maximum Kerr lensing is that in the cascaded process energy is transferred to the latter part of the pulse due to the lower group velocity of the second harmonic pulse. In figure 4.14, the results of simulations showing the difference in cascaded Kerr lensing between the case of GVM and the case of no GVM are shown.

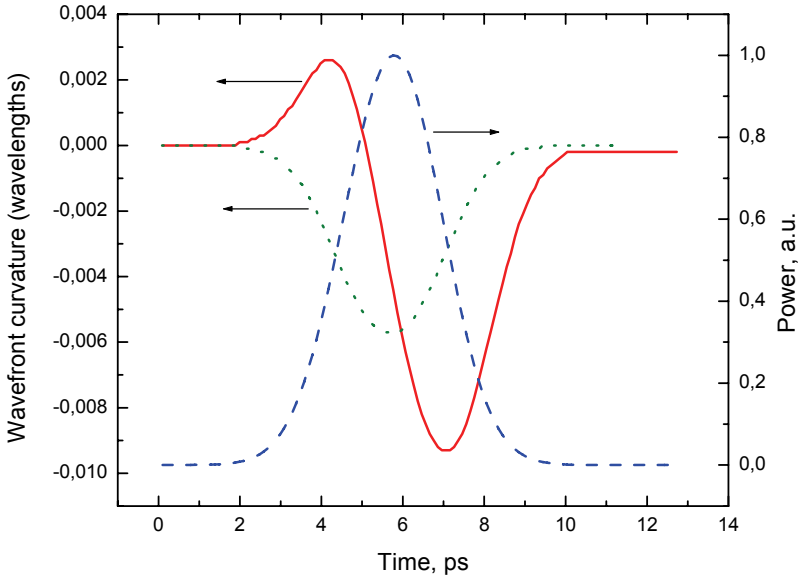

Figure 4.14. Kerr lensing with (solid) and without (dotted) GVM. The pulse profile (dashed) is included.

The beneficial effect of GVM in terms of pulse shortening is very different from the case of nonlinear mirror mode locking; where the GVM normally sets the limit to how short pulses that can be generated.

4.8.2 Hybrid mode locking

Hybrid mode locking is a combined active and passive mode locking. The advantage of a hybrid scheme is that it has the short pulses attributed to passive mode locking, but with the active modulation the requirements for self-starting the passive mode locking can be relaxed. In a self-starting passively mode locked laser the pulses are built up from noise in the cavity but in a hybrid scheme they are created by the active modulation and shortened by the passive process. This also greatly simplifies finding the mode locked region and maintaining stable operation.

In article [II] a hybrid scheme is realised with a single intracavity element, a partially poled KTP crystal. A sinusoidal electric field over the bulk part of the crystal provides a phase modulation of 0.04π by the electro-optic effect. The nonlinear crystal was kept at an elevated temperature providing a phase mismatch product ΔkL close to 2π in the periodically poled part of the crystal. The negative Kerr lens provided by the cascaded second interaction decreases the beam size at the hard aperture and improves the overlap with the pump beam at the laser crystal. This constitutes the passive mode locking. The laser is depicted in figure 4.15 and full details on distances and cavity elements are given in the article.

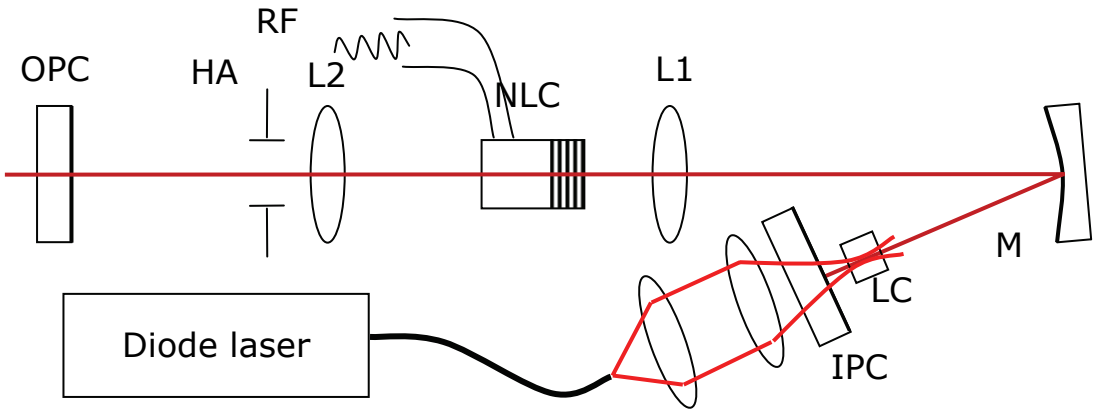

Fig. 4.15. IPC – input coupler, LC – 3 mm 0.5% doped Nd:YVO4 laser crystal, M – 750 mm radius folding mirror, L1 – 50 mm lens, L2 – 100 mm lens, NLC – partially poled KTP nonlinear crystal, RF – radio frequency voltage, HA – hard aperture, OPC – 95% reflecting output coupler. The full cavity length is 1575 mm.

In figure 4.16 the oscilloscope traces of the applied modulation and the photodiode signal monitoring the laser output power are shown. The laser keeps mode locking when the active modulation is turned off, as can be seen at the time positions of 0 s and 6 s. This shows that when mode locked the passive modulation is enough to keep mode locking. At the approximate times 2 s and 8 s the intracavity beam was momentarily blocked and the laser went into the CW regime. When the modulation was turned on again the mode locking resumed, which shows that the phase modulation provides regenerative action.

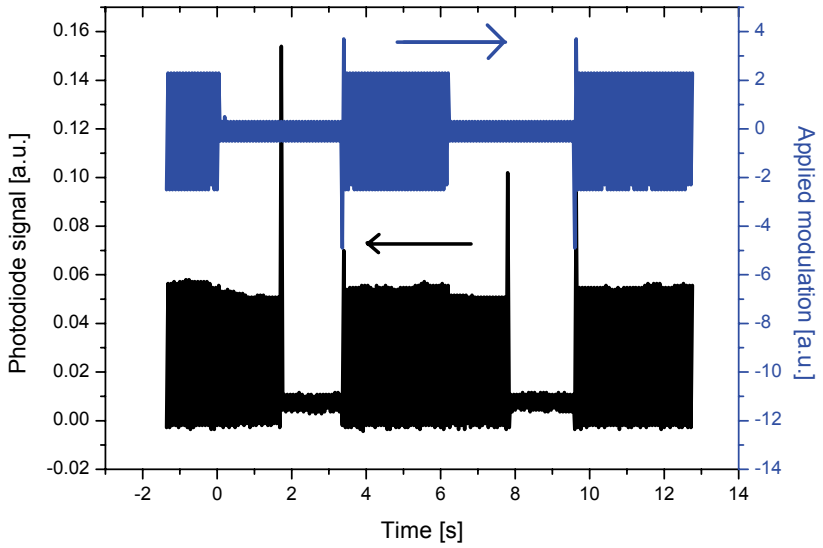

Figure 4.16. Oscilloscope traces of the applied modulation (upper curve) and the optical power of the laser (lower curve).

When pumped by 5.3 W of absorbed power the laser emitted 350 mW of stable mode locked power. The FWHM pulse lengths, shown in figure 4.17 (a), were measured with non-collinear intensity autocorrelation. The pulses were found to be 6.9 ps with the active modulation on and 7.5 ps with the active modulation off, assuming sech^2 pulse shapes. The FWHM spectral bandwidth was found to be 0.235 nm in both cases, which implies time bandwidth products of 0.43 and 0.47.

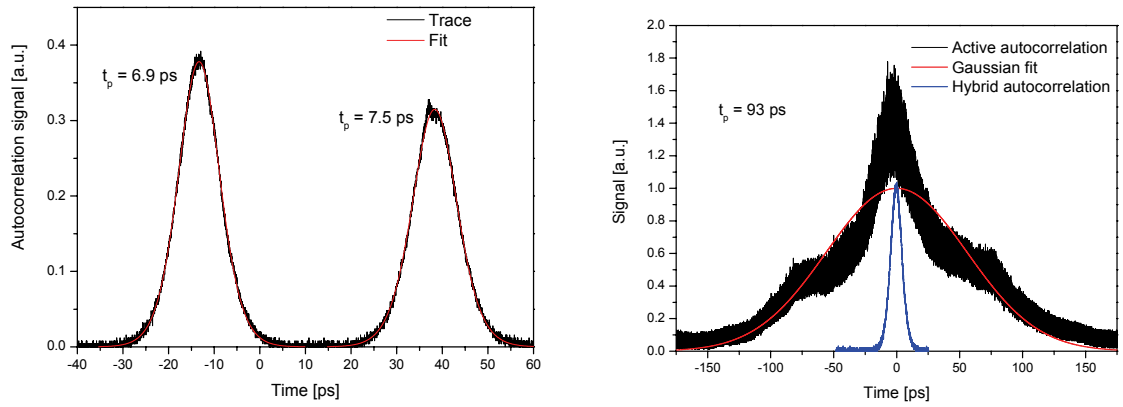

(a) (b)

Figure 4.17. (a) Intensity autocorrelation traces for the hybrid laser mode locked with the electro-optic modulation present (left-hand trace) and mode locked with the cascaded Kerr lensing only (right-hand trace). (b) Intensity autocorrelation traces. The long pulse is from phase modulation only and the short pulse is from the hybrid scheme.

In order to find out how long the seed pulses from the active modulation were, the cavity was somewhat altered into an active only mode locked equivalent. The cavity was made less sensitive to aperture effects and the lensing produced by the nonlinear crystal was greatly reduced. The output power, the cavity length and the modulation amplitude was kept the same as before the change. The pulse length was found to be around 95 ps, applying the autocorrelation fit used for Gaussian pulses. In figure 4.17 (b) the autocorrelation trace is shown together with that of the hybrid mode locking. The active only mode locked pulse is about 14 times longer, which clearly demonstrates the pulse shortening of the hybrid scheme.

4.9 Čerenkov phase matching

Čerenkov phase matching is named after the Nobel laureate P. Čerenkov,[129] who in 1934 observed that a charged particle (most commonly an electron originating from radioactive decay), passing though a dielectric at a speed faster than the speed of light in the media, will cause coherent electromagnetic radiation at an angle that depends on the refractive index of the material.

Čerenkov phase matching does not fulfil the full vectorial phase matching condition of equation 2.36 but is a one-dimensional phase matching condition. As mentioned in paragraph 3.1, under normal dispersion the refractive index is higher for the second harmonic light than for the fundamental beam. This means that it is possible to find a direction of the second harmonic such that the phase matching condition in the direction of the fundamental beam is fulfilled

$$cos\left(\theta_i(\lambda)\right) = \frac{n(\omega,\theta_i)}{n(2\omega,\theta_i)} \qquad 4.20$$

Here θ_i is the internal angle of the Čerenkov radiation, λ is the fundamental wavelength and n is the phase refractive index. Depending on the polarizations involved n may or may not depend on θ_i. The Čerenkov interaction does not take place in bulk media, since a discontinuity smaller than the wavelength of the fundamental beam is required. This can be

provided by the nonlinear polarisation at the domain wall of a ferroelectric nonlinear crystal. Čerenkov phase matched SHG was recently generated at the domain walls of PPKTP,[130] utilising *d* coefficients normally forbidden by the crystal symmetry. In figure 4.18 Čerenkov phase matching is illustrated.

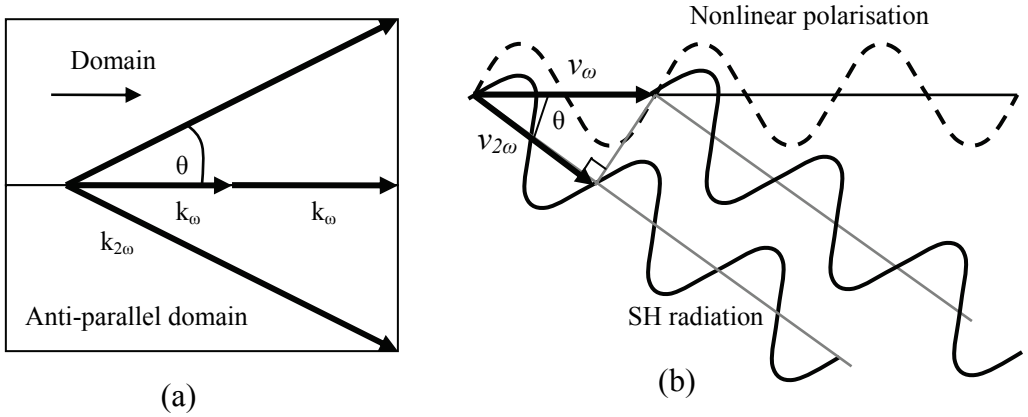

Figure 4.18. (a) Čerenkov phase matching illustrated with wave vectors. (b) Čerenkov phase matching illustrated by waves.

4.9.1 Čerenkov FROG

Performing correct measurements of fs pulses is a challenging task. Autocorrelation techniques typically involve the assumption of a pulse shape and are therefore not fully reliable. All autocorrelation methods split the pulses in two and recombine them again – either with a scanning delay line measuring pulse lengths on an average over many pulses or by using the geometry when two pulses overlap non-collinearly to facilitate single pulse measurements.[131,132]

The solution of many of the problems involved with the autocorrelation techniques is to employ the Frequency-Resolved Optical Gating (FROG) method.[133,134] A FROG is an autocorrelation technique in which the signal is spectrally resolved. With this information the intensity and phase of the pulse can be extracted. The FROG signal can be a 2D image where time is depicted on one axis and spectrum on the other. One such option is to use the temporal resolution of a single shot autocorrelator geometry combined with the spectral spread of Čerenkov phase matching, as is demonstrated in article [VI].

There are three properties that make Čerenkov phase matched SHG particularly well suited for the frequency resolved optical gating (FROG) technique. One is that the phase matched bandwidth is huge. The same nonlinear crystal can be used for pulses ranging from the visible to the mid infrared. The second is that since the direction of the second harmonic light varies with wavelength, then there is no need for a separate grating element – the nonlinear process works as an angular dispersive element. The third is that since the second harmonic is generated in a thin region at the domain wall, excellent spatial resolution can be achieved.

The geometry of the interaction employed for the FROG arrangement is shown in fig. 4.19. The fundamental pulses from a commercial Ti:Sapphire amplifier each give rise to non-phase-matched SHG in the collinear direction (NPSHG1 and NPSHG2). If there is temporal and spatial overlap, there will be non-phase-matched SFG (NPSFG) in the non-collinear direction. This could be used for an independent temporal autocorrelation measurement. When there is a domain wall in the overlap region, there will be symmetric pattern of Čerenkov phase matched SHG and SFG (ČSHG1, ČSHG2 and ČSFG) emitted from the crystal. Either of the sum frequency Čerenkov beams can be used for the measurement.

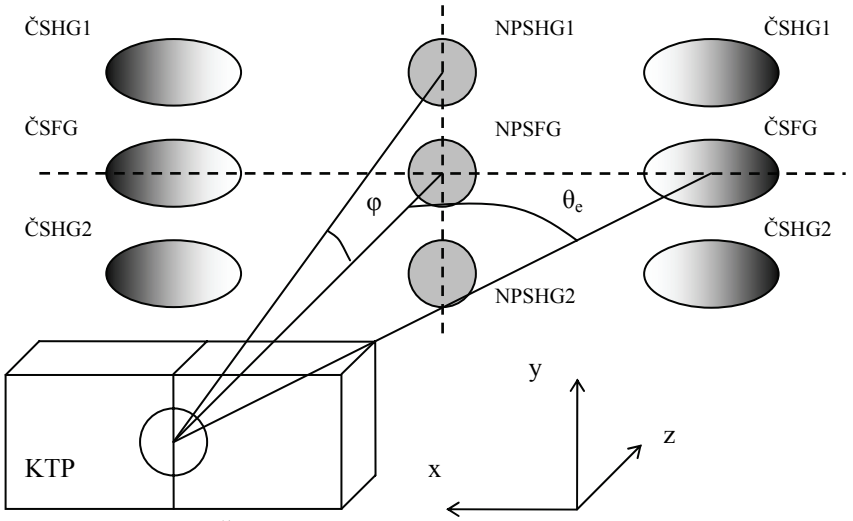

Figure 4.19. The geometry of the Čerenkov phase matched interaction used in the FROG arrangement. The fundamental pulses propagate in the y-z plane in the directions of NPSHG1 and NPSHG2. The graded spots indicate angular dispersion.

In the experiment we utilise the d_{11} nonlinear coefficient in a domain wall of KTP. This represents a forbidden interaction in the bulk crystal, but at and close to the wall the coefficient is nonzero with a value of $d_{11} = 0.45$ pm/V.[130] The Cerenkov phase matching condition of equation 4.20 was solved for x-polarised interacting waves and the result in terms of external angle θ_e and angular dispersion is shown in figure 4.20.

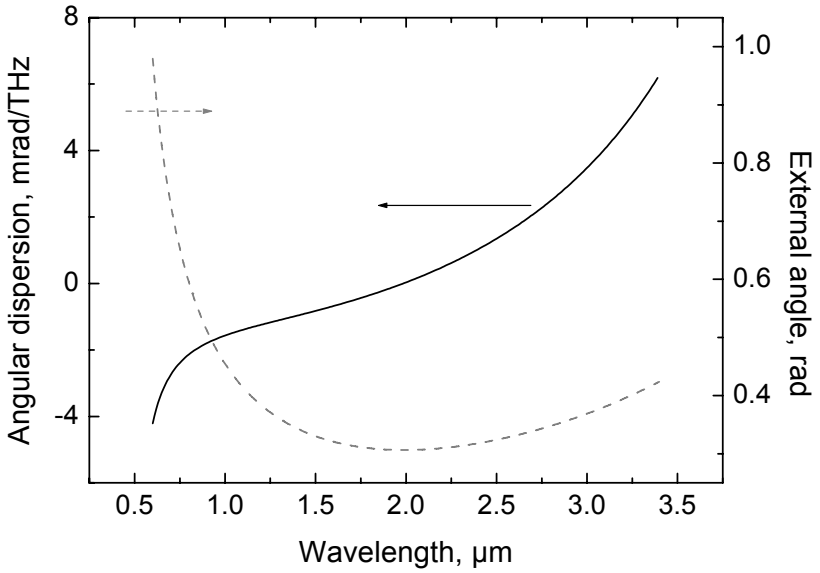

Figure 4.20. Angular dispersion and external angles of Čerenkov radiation in KTP.

The temporal domain is imaged by a cylindrical lens onto a CCD array and the angularly spread spectral content is transformed into a spatial distribution by a cylindrical Fourier transform lens. Calibration in the time domain was achieved by delaying one of the pulses by a series of fixed delay times and correlating the movement of the peak with the autocorrelation trace. The time scale was found to be 2.4 fs per pixel. In the spectral domain, the scale and the central value was obtained by comparing the Čerenkov SFG trace on the

CCD array with the self-convolution of an independently measured fundamental spectrum. The spectral scale was found to be 0.036 nm per pixel.

In the experiment we used pulses from a commercial Ti:Sapphire generative amplifier. The complex electric field of the pulses was retrieved from the FROG traces by the general projections algorithm.[135] In the upper half of figure 4.21 (a), (b) and (c) the experimental FROG traces are shown for the cases of 8, 9 and 10 roundtrips in the amplifier. The retrieved intensities and phases as functions of time are shown below their respective FROG trace. The compression following the amplifier was not changed between the three measurements. Normally the amplifier is used with 9 round trips and this also proved to be the setting of the shortest pulse with a FWHM pulse length of 170 fs and a time bandwidth product of 0.503. In the case of 10 roundtrips the pulse was longer with a significant chirp due to the normal dispersion of the extra round trip in the amplifier and using only 8 roundtrips in the amplifier also produced a longer pulse. This was chirped with opposite sign due to too much anomalous dispersion in the compression stage. More details and numbers can be found in the article [VI].

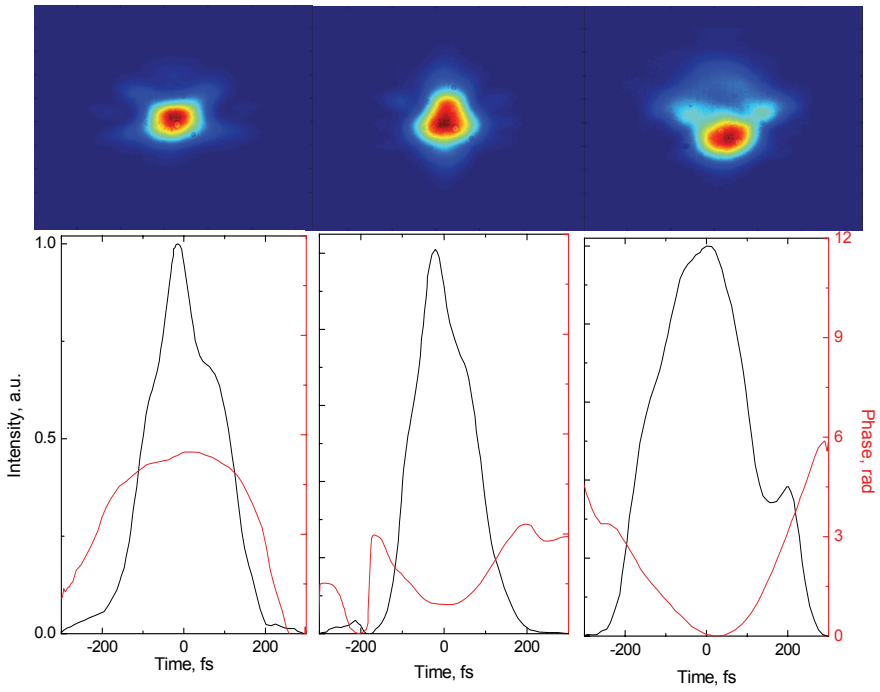

Figure 4.21. Experimental FROG traces (top row) and retrieved intensity and phase as functions of time (bottom row) for 8 (a), 9 (b) and 10 (c) roundtrips in the regenerative amplifier. In the FROG traces vertical and horizontal axes correspond to wavelength and time, respectively.

Chapter 5

Summary

The thesis work has been devoted to short optical pulses in engineered nonlinear media. In the experiments, we have demonstrated several new uses for the combination of short pulses in structured nonlinear media.

We have demonstrated two lasers, passively mode-locked by cascaded Kerr lensing in periodically poled KTP. The cascaded Kerr lensing was negative in both lasers, contrary to the case of the third order interaction. In the first laser with a fully passive scheme we show by numerical calculations that the interplay between the cavity and the group velocity mismatch causes Kerr lensing of the opposite sign in the leading part of the pulse. This effect, combined with the hard or soft cavity apertures, provide a very strong pulse shortening mechanism. The pulse length of 2.8 ps is among the shortest reported for this laser crystal and the mode locked bandwidth of 0.62 nm is about six times larger than the bandwidth for continuous operation.

The second laser had a partially poled KTP crystal close to an intracavity focus. A sinusoidal electric field over the bulk part provided phase modulation due to the electro-optic effect. The pulses generated by this active modulation were around 95 ps and they seeded the passive mode locking. A periodically poled part of the crystal together with a hard aperture provided the cascaded Kerr lens mode locking, which shortened the pulses by a factor of 14 down to pulse lengths of 6.9 ps. When the laser was passively mode locked the active modulation could be turned off without loss of mode locking. Equally significant was the fact that the passive mode locking would start from the continuous wave regime on the on-set of the active modulation. Furthermore, the active modulation greatly simplified the process of finding the parameters for passive modulation.

Frequency conversion of short pulses in periodically poled media is a process that in general is very much affected by the group velocity mismatch between the fundamental wave and the second harmonic light. This effect is less detrimental if the interaction length is short, which can be achieved by tight focussing. We demonstrated 64% second harmonic single pass conversion efficiency of the femtosecond pulses from a Yb:KYW laser. We further investigated how different focussing conditions affect the second harmonic pulse length and peak power, noting that the optimum focussing depends on the application at hand.

Quasi phase matching offers added functionality of the nonlinear crystal. One of the lesser known features is that it is possible to phase match second harmonic generation simultaneously for several different nonlinear coefficients. We demonstrated this in PPKTP and showed that polarization of the resulting dual-polarization second harmonic could be tuned both by temperature and by changing the polarization of the fundamental beam.

One problem of periodically poled crystals has been that the structure quality can vary over the sample. We demonstrated a structure quality measurement in three dimensions, utilizing the group velocity mismatch of the short fundamental pulses in a type II phase matched second harmonic generation.

In the final experiment we demonstrated a new frequency resolved optical gating method that used Čerenkov phase matched second harmonic generation at a domain wall of KTP. With this technique the intensity and phase can be retrieved for single pulses. Furthermore, the method samples the beam in a thin region at the domain wall, hereby offering high spatial resolution.

The experiments performed in this thesis work clearly demonstrates the merits of combining short pulses with designed nonlinear media.

Chapter 6

Description of original work and author contributions

Article I

Generation of 2.8 ps pulses by mode-locking a Nd:$GdVO_4$ laser with defocusing cascaded Kerr lensing in periodically poled KTP
S. J. Holmgren, V. Pasiskevicius, and F. Laurell

In this experiment we demonstrated cascaded Kerr lens mode locking of a Nd:$GdVO_4$ laser realized with a periodically poled KTP crystal. The interplay between the cavity and the group velocity dispersion caused a strong pulse shortening effect, resulting in 2.8 ps short pulses and a mode locked bandwidth of 0.62 nm.

Contributions by the author: The candidate designed and built the laser and had the main responsibility for the experiment. V. Pasiskevicius and the candidate analysed the results and wrote the article.

Article II

Active and passive hybrid mode-locking of a Nd:YVO_4 laser with a single partially poled KTP crystal
S. J. Holmgren, A. Fragemann, V. Pasiskevicius, and F. Laurell

Here we realised a hybrid mode locking scheme with a single intracavity element. The partiallly poled KTP crystal had a bulk part with active phase modulation utilizing the electro-optic effect and a periodically poled part with cascaded Kerr lensing providing passive mode locking. The active mode locking provided pulses that were shortened by a factor of 14 by the passive mode locking and when passively mode locked, the active modulation could be turned off with out loosin the mode locked action.

Contributions by the author: The candidate designed and built the laser and had the main responsibility for the experiment. The candidate also wrote the article.

Article III

Efficient Doubling of Femtosecond Pulses in Aperiodically and Periodically Poled KTP Crystals
A. A. Lagatsky, C. T. A. Brown, W. Sibbett, S. J. Holmgren, C. Canalias, V. Pasiskevicius, and F. Laurell

In this experiment we demonstrate efficient single pass second harmonic generation of the fs pulses from a Yb:KYW laser. The conversion efficiency was up to 64% and the effect of focusing on parameters as conversion efficiency, second harmonic peak power and second harmonic pulse length was studied for different pump focusing conditions.

Contributions by the author: The candidate designed the nonlinear crystals and took part in the experiments as well as the discussion related to the writing. C. Canalias fabricated the crystals used and A. Lagatsky wrote the article.

Article IV

Simultaneous second-harmonic generation with two orthogonal polarization states in periodically poled KTP
V. Pasiskevicius, S. J. Holmgren, S. Wang, and F. Laurell

Here we show a feature of quasi phase matching that is not available for birefringent phase matching, namely the possibility to utilize several nonlinear coefficients simultaneously for the generation of dual-polarization second harmonic light.

Contributions by the author: The candidate participated in the experiment and in the discussions related to the writing of the article. V. Pasiskevicius wrote the article.

Article V

Three-dimensional characterization of the effective second-order nonlinearity in periodically poled crystals
S. J. Holmgren, V. Pasiskevicius, S. Wang, and F. Laurell

In this experiment we demonstrated a new, three-dimensional characterization technique for periodically poled crystals. The method is based on group velocity mismatch between the two polarizations of the fundamental pulses in a type II second harmonic generation arrangement using fs pulses.

Contributions by the author: The candidate participated in the experiment and in the discussions and wrote the article together with V. Pasiskevicius.

Article VI

Ultrashort single-shot pulse characterization with high spatial resolution using localized nonlinearities in ferroelectric domain walls
S. J. Holmgren, C. Canalias, and V. Pasiskevicius

Here we show the use of nonlinearities at the domain walls in a single shot frequency resolved optical gating arrangement. The principle is based on Čerenkov phase matched second harmonic generation and from the CCD traces the temporal pulse intensity and phase could be retrieved. Furthermore, the method samples a thin region along the domain wall, hereby offering a high spatial resolution.

Contributions by the author: The candidate and V. Pasiskevicius designed and performed the experiment. C. Canalias provided the crystals. The candidate contributed to the article that V. Pasiskevicius wrote.

References

1. M. Born and E. Wolf, "Principles of Optics", 7th ed., Cambridge University Press, UK, (1999)
2. J. P. Gordon, H. J. Zieger, and C. H. Townes, Phys. Rev. **95**, 282 (1954)
3. J. P. Gordon, H. J. Zieger, and C. H. Townes, Phys. Rev. **99**, 1264 (1955)
4. A. L. Schawlow and C. H. Townes, Phys. Rev. **112**, 1940 (1958)
5. T. H. Maiman, Nature **187**, 493 (1960)
6. L. F. Johnson, G. D. Boyd, K. Nassau, and R. R. Soden, Phys. Rev. **126**, 1406 (1962)
7. A. Javan, W. R. Bennett, Jr., and D. R. Herriott, Phys. Rev. Lett. **6**, 106 (1961)
8. R. N. Hall, G. E. Fenner, J. D. Kingsley, T. J. Soltys, and R. O. Carlson, Phys. Rev. Lett. **9**, 366 (1962)
9. C. J. Koester and E. Snitzer, Appl. Opt. **3**, 1182 (1964)
10. L. E. Hargrove, R. L. Fork, and M. A. Pollack, Appl. Phys. Lett. **5**, 4 (1964)
11. F. J. McClung and R. W. Hellwarth, J. Appl. Phys. **33**, 828 (1962)
12. P. Franken, A. Hill, C. Peters, and G. Weinreich, Phys. Rev. Lett. **7**, 118 (1961)
13. B. A. Lengyel, Am. J. Phys. **34**, 903 (1966)
14. O. Svelto, "Principles of Lasers", 4th ed., Plenum Press, USA (1998)
15. A. E. Siegman, "Lasers",University Science Books, USA (1986)
16. A. Yariv, "Quantum Electronics", 3rd ed., John Wiley & Sons, USA (1989)
17. W. Koechner, "Solid-State Laser Engineering", 5th ed., Springer, Germany (1999)
18. W. T. Silfvast, "Laser fundamentals", 2nd ed., Cambridge University Press, UK (2004)
19. A. G. Fox and T. Li, Bell Syst. Tech. J. **40**, 453 (1961)
20. H. Kogelnik and T. Li, Appl. Opt. **5**, 1550 (1966)
21. M. A. Bandres and J. C. Gutiérrez-Vega, Opt. Lett. **29**, 144 (2004)
22. G. Goubau and F. Schwering, IRE Trans. on Antennas and Propagation **9**, 248 (1961)
23. I. Kimel and L. R. Elias, IEEE J. Quant. Electron. **29**, 2562 (1993)
24. A. E. Siegman, Proc. SPIE **1868**, 2 (1993)
25. ISO 11146, Laser and laser related equipment-Test methods for laser beam widths, divergence angles and beam propagation ratios: ISO 11146-1:2005, Part 1: Stigmatic and simple astigmatic beams; ISO11146-2:2005, Part 2: General astigmatic beams; ISO/TR 11146-3:2004, Part 3: Intrinsic and geometrical laser beam classification, propagation, and details of test method; ISO/TR 11146-3:2004/Cor1:2005, International Organization for Standardization, Switzerland, (2005)
26. P. A. Belanger, Opt. Lett. **16**, 196 (1991)
27. M. J. Bastiaans, J. Opt. Soc. Am. **69**, 1710 (1979)
28. G. Nemes and A. E. Siegman, J. Opt. Soc. Am. A **11**, 2257 (1994)
29. C. Gao, H. Laabs, H. Weber, T. Brand, and N. Kugler, Opt. and Quant. Electron. **31**, 1207 (1999)
30. J.-C. Diels and W. Rudolph, "Ultrashort Laser Pulse Phenomena", Academic Press, USA (1996)
31. R. C. Hilborn, Am. J. Phys. **50**, 982 (1982)
32. G. Karlsson, "Diode-pumped Er-Yb lasers for eye-safe applications", PhD thesis, ISBN 91-7283-455-2, Royal Institute of Technology, Sweden (2003)
33. S. Bjurshagen, "Diode-pumped rare-earth-doped quasi-three-level lasers", PhD thesis, ISBN 91-7178-220-6, Royal Institute of Technology, Sweden (2005)
34. A. Minassian, B. Thompson and M.J. Damzen, Appl. Phys. B **76**, 341 (2003)
35. W. Sibbett, in "Laser Sources and Applications", ed. A. Miller and D. M. Finlayson, SUSSP Publications and Institute of Physics Publishing, UK (1996)
36. T. Uchida, IEEE J. Quantum Electron. **1**, 336 (1965)
37. S. E. Harris and R. Targ, Appl. Phys. Lett. **5**, 202 (1964)
38. W. C. Henneberger and H. J. Schulte, J. Appl. Phys. **37**, 2189 (1966)
39. R. L. Fork, B. I. Greene, and C. V. Shank, Appl. Phys. Lett. **38**, 671 (1981)
40. H. W. Mocker and R. J. Collins, Appl. Phys. Lett. **7**, 270 (1965)
41. A. J. DeMaria, D. A. Stetser, and H. Heynau, Appl. Phys. Lett. **8**, 174 (1966)
42. P. W. Smith, Y. Silberberg, and D. A. B. Miller, J. Opt. Soc. Am. B **2**, 1228 (1985)
43. U. Keller, K. J. Weingarten, F. X. Kartner, D. Kopf, B. Braun, I. D. Jung, R. Fluck, C. Honninger, N. Matuschek and J. Aus der Au, IEEE J. Sel. Topics Quantum. Electron. **2**, 435 (1996)
44. G. New, IEEE J. Quantum. Electron. **10**, 115 (1974)
45. L. F. Mollenauer and R. H. Stolen, Opt. Lett. **9**, 13 (1984)

46. U. Morgner, F. X. Krtner, S. H. Cho, Y. Chen, H. A. Haus, J. G. Fujimoto, E. P. Ippen, V. Scheuer, G. Angelow, and T. Tschudi, Opt. Lett. **24**, 411 (1999)
47. D. H. Sutter, G. Steinmeyer, L. Gallmann, N. Matuschek, F. Morier-Genoud, U. Keller, V. Scheuer, G. Angelow, and T. Tschudi, Opt. Lett. **24**, 631 (1999)
48. D. E. Spence, P. N. Kean, and W. Sibbett, Opt. Lett. **16**, 42 (1991)
49. F. X. Kärtner, N. Matuschek, T. Schibli, U. Keller, H. A. Haus, C. Heine, R. Morf, V. Scheuer, M. Tilsch, and T. Tschudi, Opt. Lett. **22**, 831 (1997)
50. R. L. Fork and O. E. Martinez, Opt. Lett. **9**, 150 (1984)
51. K. A. Stankov and J. Jethwa, Opt. Commun. **66**, 41 (1988)
52. K. A. Stankov, Appl. Phys. B **45**, 191 (1988)
53. V. Couderc, O. Guy, E. Roisse, A. Barthelemy, Electron. Lett. **34**, 672 (1998)
54. S. Saltiel, K. Koynov and I. Buchvarov, Appl. Phys. B **63**, 371 (1996)
55. L. Lefort and A. Barthelemy, Opt. Lett. **20**, 1749 (1995)
56. S. Louis, V. Couderc, F. Louradour, P. Faugeras and A. Barthélémy, J. Opt. A: Pure Appl. Opt. **3**, 139 (2001)
57. G. Cerullo, S. De Silvestri, A. Monguzzi, D. Segala, and V. Magni, Opt. Lett. **20**, 746 (1995)
58. R. DeSalvo, D. J. Hagan, M. Sheik-Bahae, G. I. Stegeman, E. W. Van Stryland, and H. Vanherzeele, Opt. Lett. **17**, 28 (1992)
59. Y. R. Shen, "The Principles of Nonlinear Optics", John Wiley & Sons, USA (1984)
60. P. N. Butcher and D. Cotter, "The Elements of Nonlinear Optics", Cambridge University Press, UK (1990)
61. R. L. Sutherland, "Handbook of Nonlinear Optics", 2nd ed., Marcel Dekker, USA (2003)
62. R. W. Boyd, "Nonlinear Optics", Academic Press, USA (1992)
63. O. S. Heavens, R. W. Ditchburn, "Insight into Optics", Wiley, UK (1991)
64. D. A. Kleinman, Phys. Rev. **126**, 1977 (1962)
65. J. E. Midwinter and J. Warner, Brit. J. Appl. Phys. **16**,1135 (1965)
66. F. Zernike and J. E. Midwinter, "Applied Nonlinear Optics", John Wiley & Sons, USA (1973)
67. A. Ashkin, G. D. Boyd, and J. M. Dziedzic, Phys. Rev. Lett. **11**, 14 (1963)
68. J. Ducuing and N. Bloembergen, Phys. Rev. **133**, A1493 (1964)
69. S. Helmfrid, G. Arvidsson, J. Opt. Soc. Am. B **8**, 2326 (1991)
70. W. P. Risk, T. R. Gosnell, A. V. Nurmikko "Compact blue-green lasers", Cambridge University Press, UK (2003)
71. P. D. Maker, R. W. Terhune, M. Nisenoff, and C. M. Savage, Phys. Rev. Lett. **8**, 21 (1962)
72. J. A. Giordmaine, Phys. Rev. Lett. **8**, 19 (1962)
73. A. Yariv and P. Yeh, "Optical Waves in Crystals", John Wiley & Sons, USA (1984)
74. D. A. Kleinman, Phys. Rev. **128**, 1761 (1962)
75. G. D. Boyd, A. Ashkin, J. M. Dziedzic, and D. A. Kleinman, Phys. Rev. **137**, 305 (1965)
76. M. V. Hobden, J. Appl. Phys. **38**, 4365 (1967)
77. J. A. Armstrong, N. Bloembergen, J. Ducuing, and P. S. Pershan, Phys. Rev. **127**, 1918 (1962)
78. P. G. Kazansky and V. Pruneri, J. Opt. Soc. Am. B **14**, 3170 (1997)
79. P. A. Franken and J. F. Ward, Rev. Modern Phys. **35**, 23 (1963)
80. A. Szilagyi, A. Hordvik, and H. Schlossberg, J. Appl. Phys. **47**, 2025 (1976)
81. D. E. Thompson, J. D. McMullen, and D. B. Anderson, Appl. Phys. Lett. **29**, 113 (1976)
82. L. Gordon, G. L. Woods, R. C. Eckardt, R. R. Route, R. S. Feigelson, M. M. Fejer and R. L. Byer, Electron. Lett. **29**, 1942 (1993)
83. T. Skauli, K. L. Vodopyanov, T. J. Pinguet, A. Schober, O. Levi, L. A. Eyres, M. M. Fejer, J. S. Harris, B. Gerard, L. Becouarn, E. Lallier, and G. Arisholm, Opt. Lett. **27**, 628 (2002)
84. B. F. Levine, C. G. Bethea, and R. A. Logan, Appl. Phys. Lett. **26**, 375 (1975)
85. D. Feng, N. B. Ming, J. F. Hong, Y. S. Yang, J. S. Zhu, Z. Yang, and Y. N. Wang, Appl. Phys. Lett. **37**, 607 (1980)
86. J. Webjörn, F. Laurell, and G. Arvidsson, J. Lightwave Technol. **7**, 1597 (1989)
87. M. Yamada and K. Kishima, Electron. Lett. **27**, 828 (1991)
88. M. Yamada, N. Nada, M. Saitoh, and K. Watanabe, Appl. Phys. Lett. **62**, 435 (1993)
89. J. Webjörn, V. Pruneri, P. S. J. Russel, J. R. M. Barr, and D. C. Hanna, Electron. Lett. **30**, 894 (1994)
90. Q. Chen and W. P. Risk, Electron. Lett. **30**, 1516 (1994)
91. H. Karlsson and F. Laurell, Appl. Phys. Lett. **71**, 3474 (1997)
92. H. Karlsson, "Fabrication of periodically poled crystals from the KTP family and their applications in nonlinear optics", PhD thesis, ISSN 0280-316X, Royal Institute of Technology, Sweden (1999)
93. J. Hellström, "Nanosecond optical parametric oscillators and amplifiers based on periodically poled $KTiOPO_4$", PhD thesis, ISBN 91-7283-214-2, Royal Institute of Technology, Sweden (2001)

94. C. Canalias, "Domain Engineering in $KTiOPO_4$", PhD thesis, ISBN 91-7178-152-8, Royal Institute of Technology, Sweden (2005)
95. S. Wang, "Fabrication and characterization of periodically-poled KTP and Rb-doped KTP for applications in the visible and UV", PhD thesis, ISBN 91-7178-153-6, Royal Institute of Technology, Sweden (2005)
96. D. T. Reid, J. Opt. A: Pure Appl. Opt. **5**, S97 (2003)
97. M. M. Fejer, G. A. Magel, D. H. Jundt, and R. L. Byer, IEEE J. Quantum Electron **28**, 2631 (1992)
98. F. C. Zumsteg, J. D. Bierlein, and T. E. Gier, J. Appl. Phys. **47**, 4980 (1976)
99. H. Vanherzeele and J. D. Bierlein, Opt. Lett. **17**, 982 (1992)
100. T. Y. Fan, C. E. Huang, B. Q. Hu, R. C. Eckardt, Y. X. Fan, R. L. Byer, and R. S. Feigelson, Appl. Opt. **26**, 2390 (1987)
101. K. Fradkin, A. Arie, A. Skliar, and G. Rosenman, Appl. Phys. Lett. **74**, 914 (1999)
102. K. Kato and E. Takaoka, Appl. Opt. **41**, 5040 (2002)
103. W. Wiechmann, S. Kubota, T. Fukui, and H. Masuda, Opt. Lett. **18**, 1208 (1993)
104. J. D. Bierlein and H. Vanherzeele, J. Opt. Soc. Am. B **6**, 622 (1989)
105. G. Hansson, H. Karlsson, S. Wang, and F. Laurell, Appl. Opt. **39**, 5058 (2000)
106. J. D. Bierlein and F. Ahmed, Appl. Phys. Lett. **51**, 1322 (1987)
107. G. T. Kennedy, D.T. Reid, A. Miller, M. Ebrahimzadeh, H. Karlsson, G. Arvidsson, and F. Laurell, Opt. Lett. **23**, 503 (1998)
108. K. Nassau, H. J. Levinstein, and G. M. Loiacono, Appl. Phys. Lett. **6**, 228 (1965)
109. F. Laurell, M. G. Roelofs, W. Bindloss, H. Hsiung, A. Suna, and J. D. Bierlein, J. Appl. Phys. **71**, 4664 (1992)
110. H. Karlsson, F. Laurell and L. K. Cheng, Appl. Phys. Lett. **74**, 1519 (1999)
111. J. Hellström, R. Clemens, V. Pasiskevicius, H. Karlsson, and F. Laurell, J. Appl. Phys. **90**, 1489 (2001)
112. C. Canalias, V. Pasiskevicius, F.Laurell, S. Grilli, P. Ferraro, and P. De Natale "In situ visualization of domain kinetics in flux grown KTiOPO4 by digital holography" (Submitted to Appl. Phys. Lett.)
113. S. Wang, V. Pasiskevicius, J. Hellström, F. Laurell, and H. Karlsson, Opt. Lett. **24**, 978 (1999)
114. C. Canalias, V. Pasiskevicius, A. Fragemann, and F. Laurell, Appl. Phys. Lett. **82**, 734 (2003)
115. A. Reichert and K. Betzel, J. Appl. Phys. **79**, 2209 (1996)
116. D. A. Kleinman, A. Ashkin, and G. D. Boyd, Phys. Rev. **145**, 338 (1966)
117. G. D. Boyd and D. A. Kleinman, J. Appl. Phys. **39**, 3597 (1968)
118. K. Asaumi, Appl. Phys. B **54**, 265 (1992)
119. J. J. Zondy, Opt. Commun. **81**, 427 (1997)
120. F. Librecht, J. Simons, IEEE J. Quantum Electronics **11**, 850 (1975)
121. Y. Taira, Jpn. J. Appl. Phys. **31,** L682 (1992)
122. S. M. Saltiel, K. Koynov, B. Agate, and W. Sibbett, J. Opt. Soc. Am. B **21**, 591 (2004)
123. A. A. Lagatsky, E. U. Rafailov, A. R. Sarmani, C. T. A. Brown, W. Sibbett, L. Ming, and P. G. R. Smith, Opt. Lett. **30**, 1144 (2005)
124. E. W. Van Stryland, in "Laser Sources and Applications", ed. A. Miller and D. M. Finlayson, SUSSP Publications and Institute of Physics Publishing, UK (1996)
125. F. Wise, L. Qian and X. Liu, J. Nonlinear Opt. Phys. Mat. **11**, 317 (2002)
126. G. Toci, M. Vannini, and R. Salimbeni, J. Opt. Soc. Am. B **15**, 103 (1998)
127. V. Magni, G. Cerullo and S. De Silvestri, Opt. Commun. **96**, 348 (1993)
128. http://www.sandia.gov/imrl/X1118/xxtal.htm
129. P. A. Cherenkov, Comptes Rendus Acad. Sciences USSR **2**, 451 (1934)
130. A. Fragemann, V. Pasiskevicius and F. Laurell, Appl. Phys. Lett. **85**, 375 (2004)
131. J. Janszky, G. Corradi, and R. N. Gyuzalian, Opt. Comm. **23**, 293 (1977)
132. F. Salin, P. Georges, G. Roger, and A. Brun, Appl. Opt. **26**, 4528 (1987)
133. D. J. Kane and R. Trebino, Optics Lett. **18**, 823 (1993)
134. R. Trebino, K. W. DeLong, D. N. Fittinghoff, J. N. Sweetser, M. A. Krumbügel, B. A. Richman and D. J. Kane, Rev. Sci. Instrum. **68**, 3277 (1997)
135. K. W. DeLong and R. Trebino, J. Opt. Soc. Am B **11**, 2206 (1994)